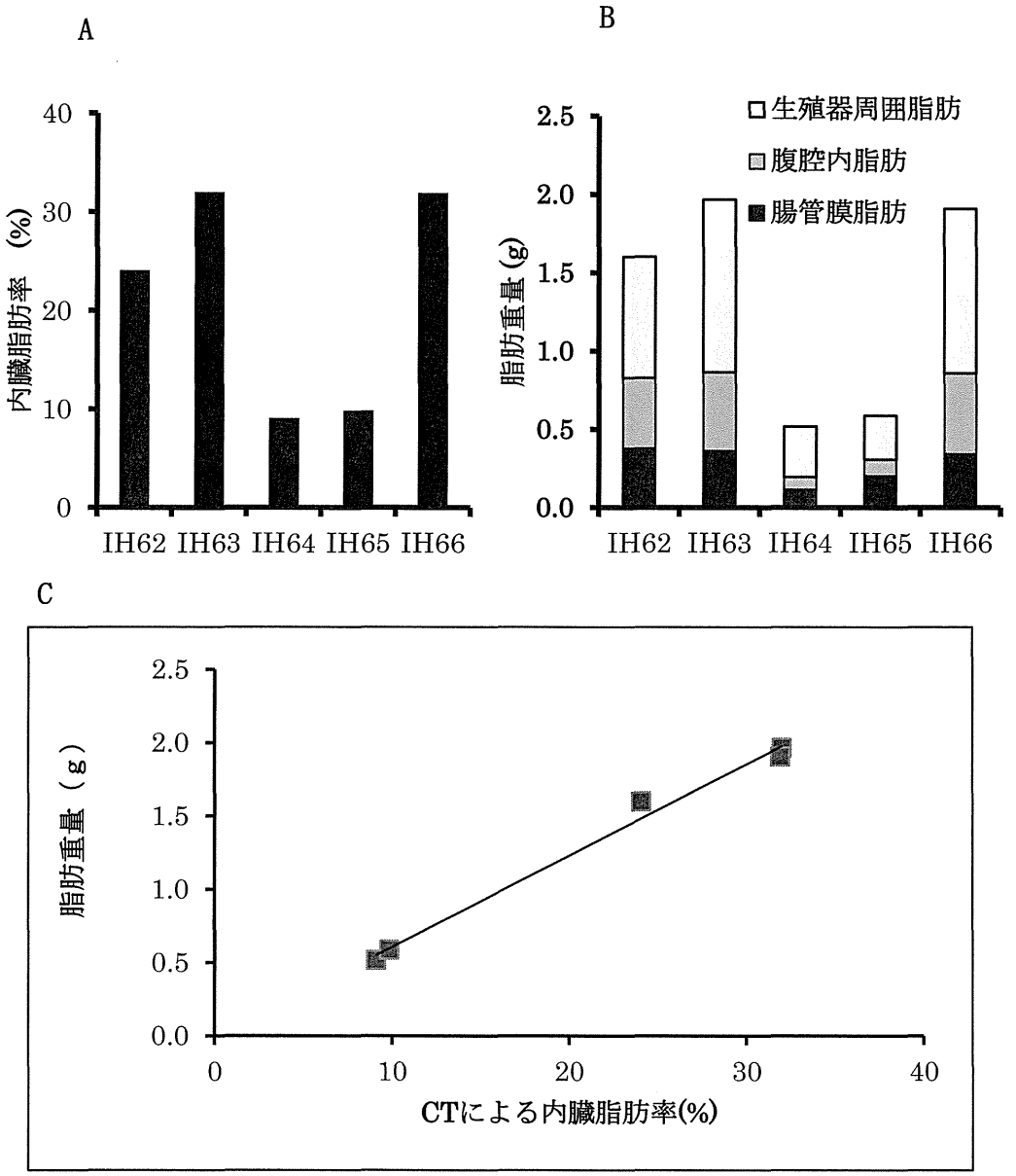

図 3.　小動物用X線 CT 装置による内臓脂肪の測定

A: CT 測定による内臓脂肪率 {脂肪率 ＝脂肪重量／(筋肉重量＋脂肪重量) X 100}

B: 生殖器周囲脂肪、腹腔内脂肪および腸管膜脂肪の重量測定値

C: CT による脂肪率 と脂肪重量の相関性

28 週齢の ApoE-KO マウス 5 例の腹部 CT より算出した内臓脂肪率と摘出した脂肪重量はよい相関を示した。

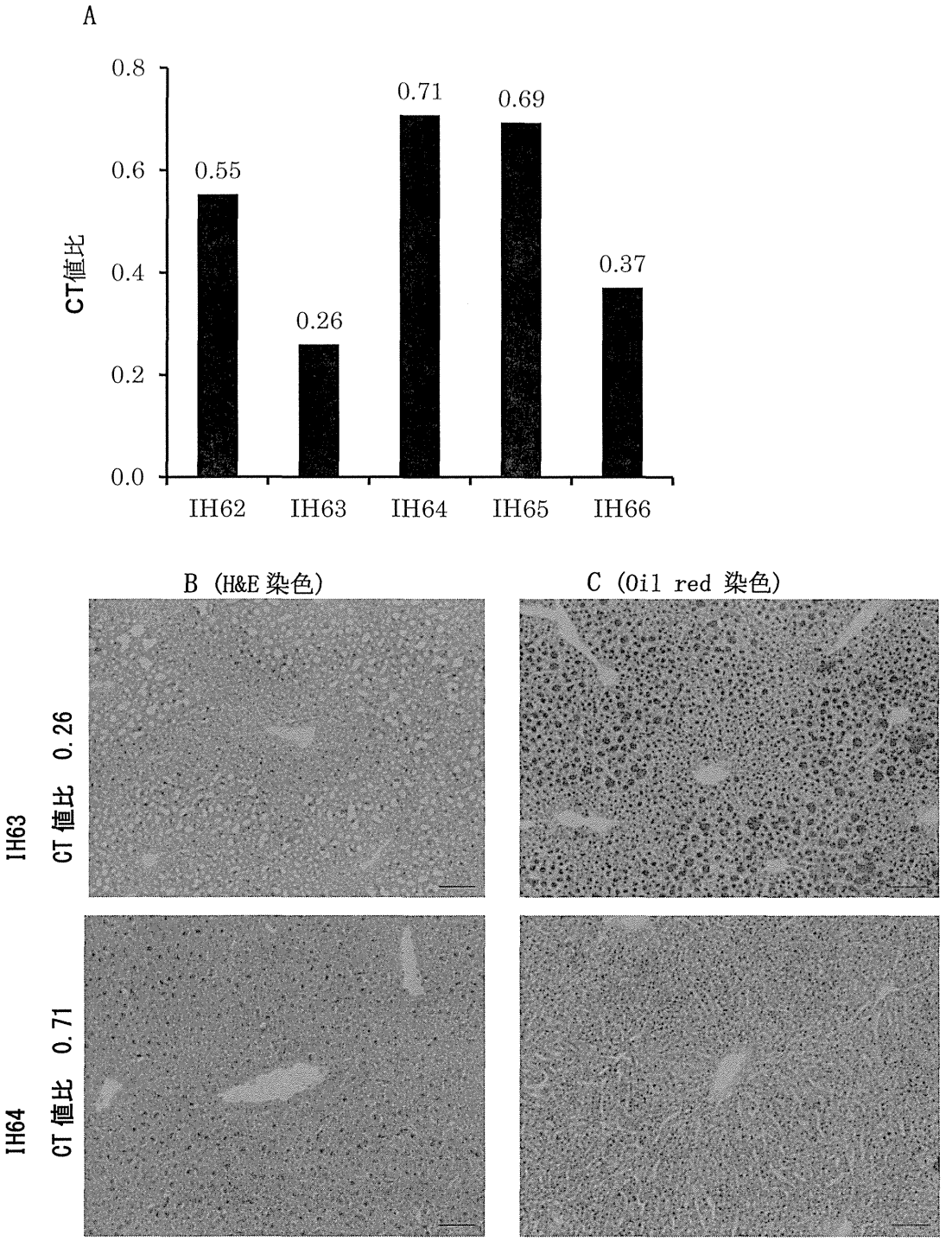

図 4.　肝臓の CT 値比と病理組織染色の比較

A: CT による肝臓の CT 値比、B: 肝臓の H&E 染色、C: 肝臓の Oil red 脂肪染色

病理組織学的に CT 値比が高値（下段 0.71)は、低値（上段 0.26)に比べて脂肪の蓄積が強い。

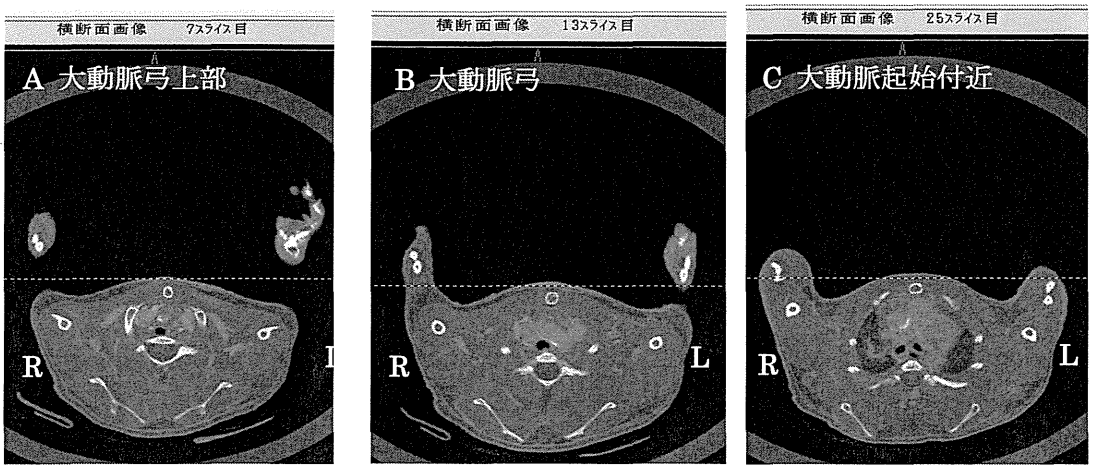

図 5.　イオパミロン静脈投与 10 分後の血管造影像

A: 大動脈弓上部　B：大動脈弓　C: 大動脈起始部付近

A～C の位置において 血管内に白い石灰化像が見られた。

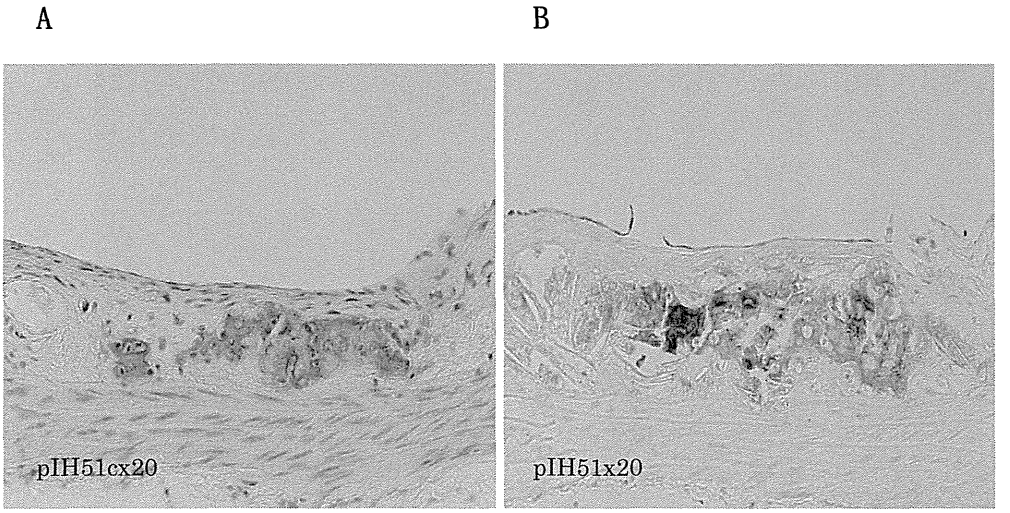

図 6.　石灰化を伴う動脈硬化病変

A: H&E 染色、　B: Kossa 反応

ApoE-KO マウスの動脈硬化病変部に、Kossa 反応陽性部位が観察され、H&E 染色での所見との関連付けが出来た。

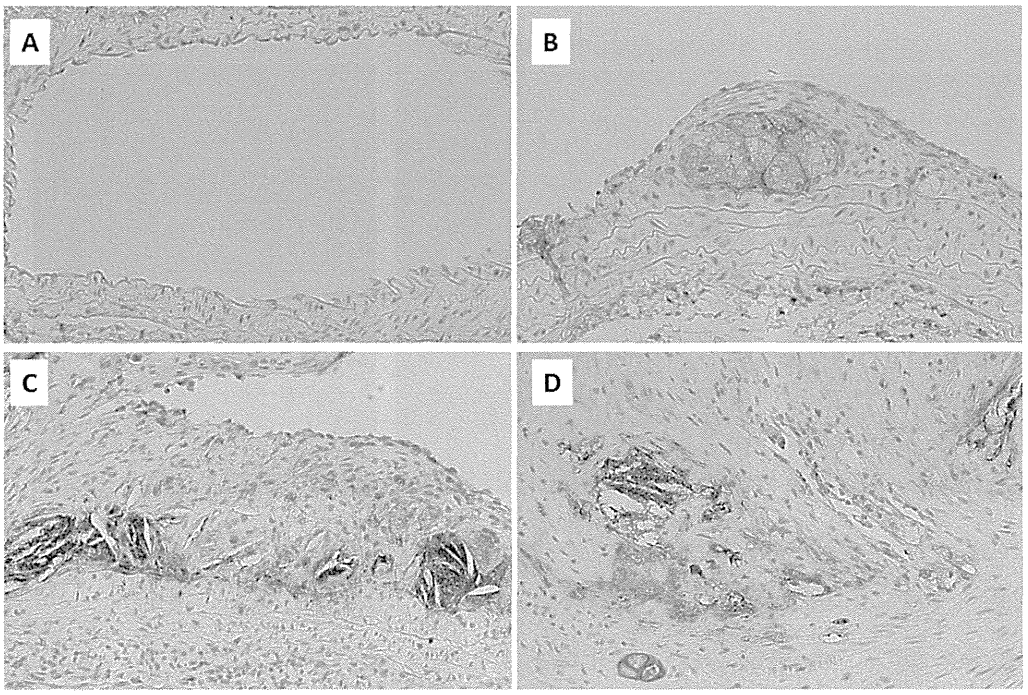

図 7.　動脈硬化病変の F4/80 陽性を示すマクロファージ

A:　Wild type マウス、 B～D: ApoE-KO マウス、 X200、 F4/80 免疫組織学的染色

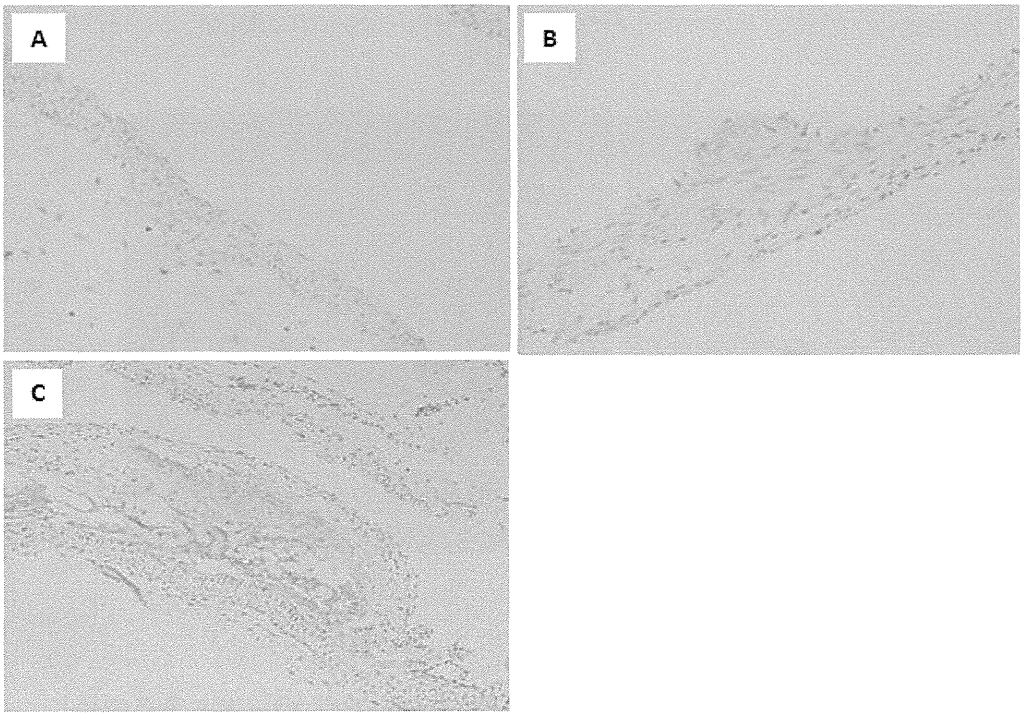

図 8.　動脈硬化病変の TIMP-1 発現

A:　Wild type マウス、 B～D: ApoE-KO マウス、X200、TIMP-1 免疫組織学的染色

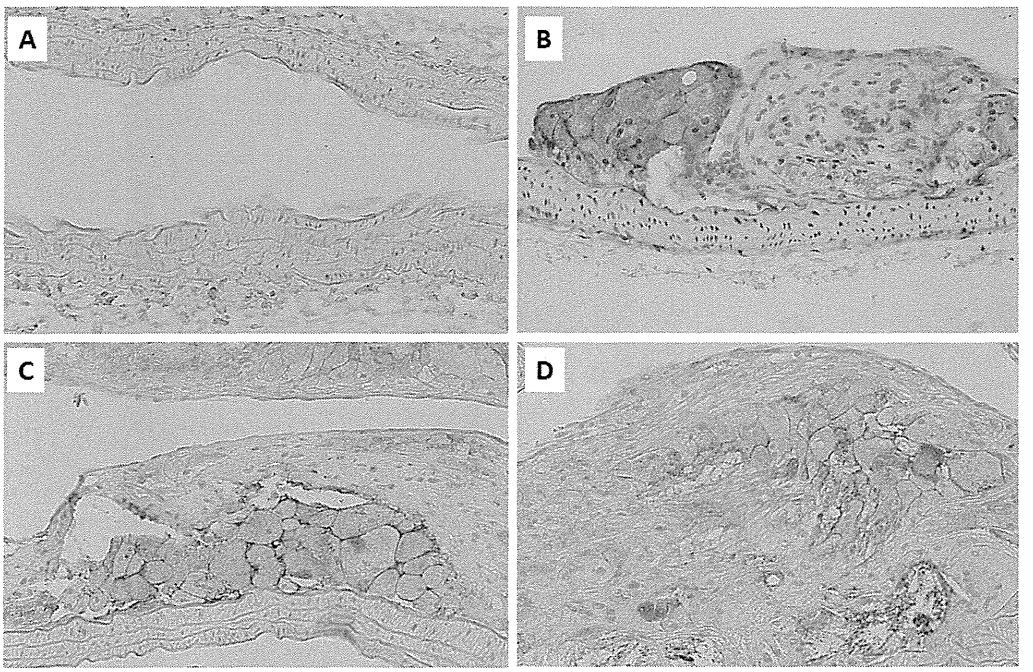

図 9.　動脈硬化病変の MMP-9 発現

A:　Wild type マウス、 B～D: ApoE-KO マウス、 X200、 MMP-9 免疫組織学的染色

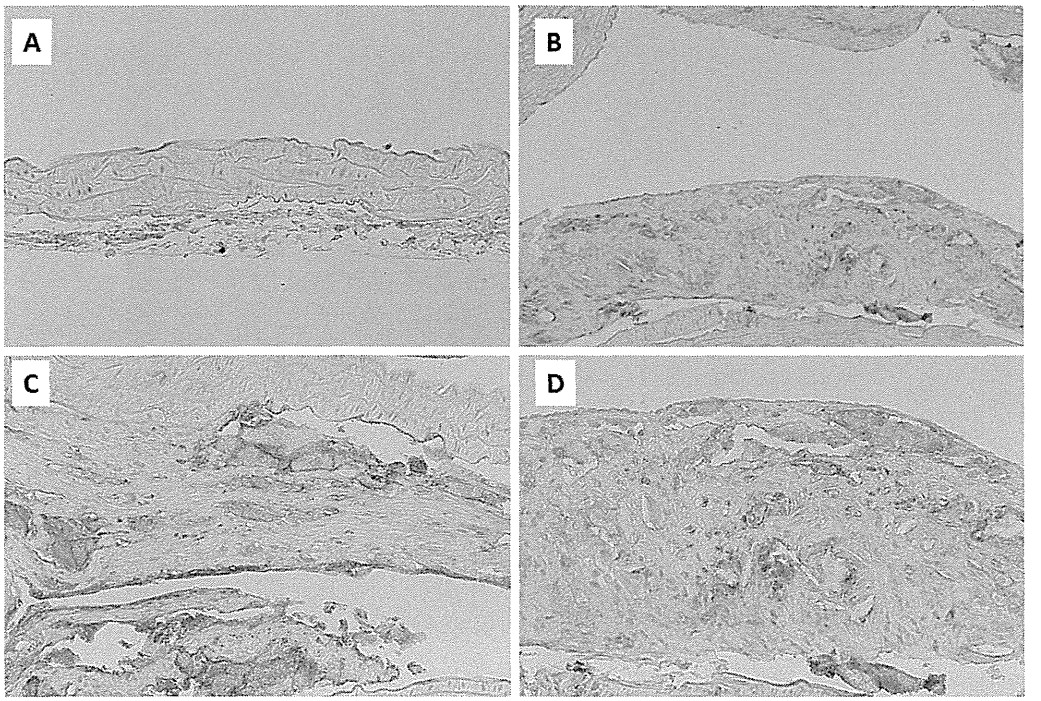

図 10.　動脈硬化病変の MMP-1/8 発現

A:　Wild type マウス、B～D: ApoE-KO マウス、X200, MMP-1/8 免疫組織学的染色

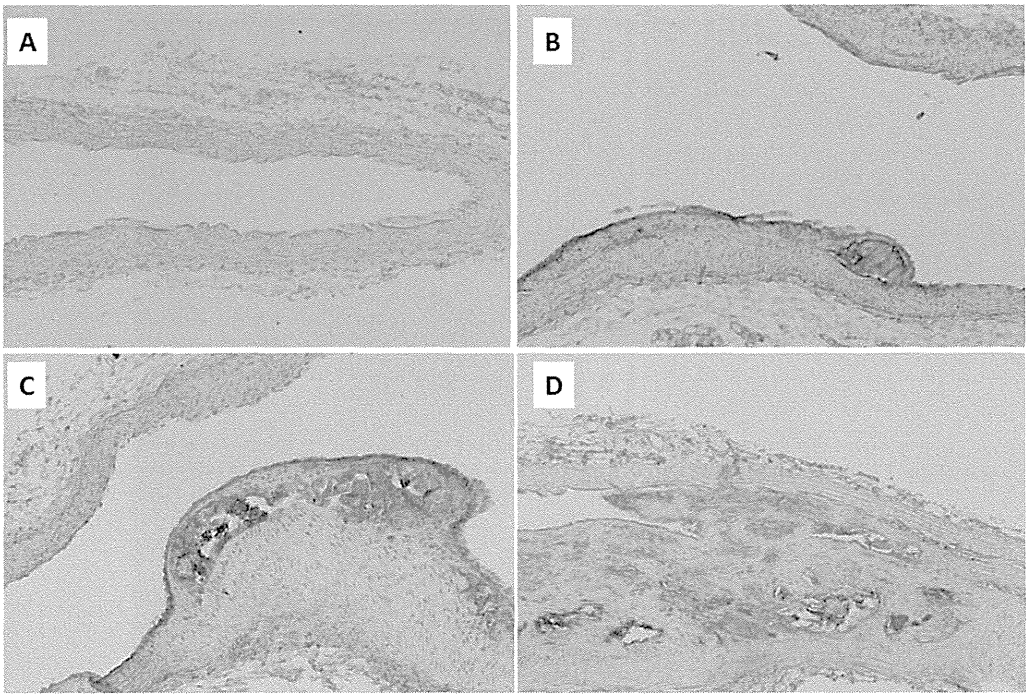

図 11.　動脈硬化病変の sLOX-1 発現

A:　Wild type マウス、 B～D: ApoE-KO マウス、X200,、sLOX-1 免疫組織学的染色

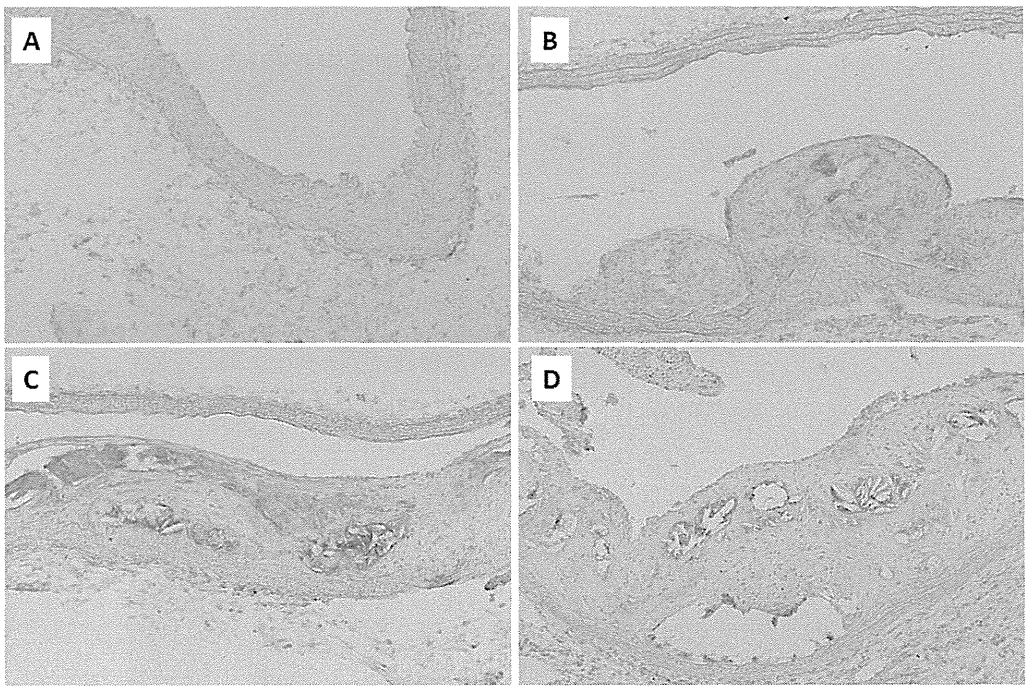

図 12.　動脈硬化病変の Cxcl16 発現

A:　Wild type マウス、B～D: ApoE-KO マウス、X200、Cxcl16 免疫組織学的染色

別紙４

研究成果の刊行に関する一覧表レイアウト

雑誌

発表者氏名	論文タイトル名	発表誌名	巻号	ページ	出版年
Yamamoto T, Yahara A, Waki R, Yasuhara H, Wada F, Harada-Shiba M, Obika S	Amido-bridged Nucleic Acids with Small Hydrophobic Residues Enhance Hepatic Tropism of Antisense Oligonucleotides *in vivo*	Org. Biomol. Chem			2015年
Hori M, Ishihara M, Yuasa Y, Makino H, Yanagi K, Tamanaha T, Kishimoto I, Kujiraoka T, Hattori H, Harada-Shiba M	Removal of plasma mature and furin-cleaved proprotein convertase subtilisin/kexin 9 (pcsk9) by low-density lipoprotein-apheresis in familial hypercholesterolemia: Development and application of a new assay for pcsk9	J. Clin. Endocrinol. Metab			2014年
Yamamoto T, Fujii N, Yasuhara H, Wada S, Wada F, Shigesada H, Harada-Shiba M, Obika S	Evaluation of Multiple-Turnover Capability of Locked Nucleic Acid Antisense Oligonucleotides in Cell-Free RNase H-Mediated Antisense Reaction and in Mice	Nucleic Acid Therapeutics	24	283-290	2014年
Yamamoto T, Obika S, Nakatani M, Yasuhara H, Wada F, Shibata E, Shibata MA, Harada-Shiba M	Locked nucleic acid antisense inhibitor targeting apolipoprotein C-III efficiently and preferentially removed triglyceride from large VLDL particles from murine plasma	European Journal of Pharmacology	723	353-359	2014年
Yuasa Y, Osaki T, Makino H, Iwamoto N, Kishimoto I, Usami M, Harada-Shiba M	Proeomic analysis of proteins eliminated by LDL-apheresis	Ther Apher Dial	18 (1)	93-102	2014年
Mori K, Kodama T, Obika S	Synthesis and Hybridization Property of a Boat-shaped Pyranosyl Nucleic Acid Containing an Exocyclic Methylene Group in the Sugar Moiety	Bioorg. Med. Chem	23	33-37	2015年
Mitsuoka Y, Fujimura Y, Waki R,Kugimiya A, Yamamoto T,Hari Y, Obika S	Sulfonamide-Bridged Nucleic Acid: Synthesis, High RNA Selective Hybridization, and High Nuclease Resistance	Org. Lett	16	5640-5643	2014年

Mori S, Morihiro K, Obika S	C5-Azobenzene-substituted 2'-Deoxyuridine-containing-oligodeoxynucleotides for Photo-switching Hybridization Ability	Molecules	19	5109-5118	2014年
Morihiro K, Kodama T, Mori S, Obika S	Photoinduced Changes in Hydrogen Bonding Patterns of 8-Thiopurine Nucleobase Analogues in a DNA Strand	Org. Biomol. Chem	12	2468-2473	2014年
Shimo T, Tachibana K, Saito K, Yoshida T, Tomita E, Waki R, Yamamoto T, Doi T, Inoue T, Kawakami J, Obika S	Design and Evaluation of 2',4'-BNA/LNA Based Splice-switching Oligonucleotides in Vitro	Nucleic Acids Res	42	8174-8187	2014年
柴田雅朗, 日下部守昭, 森本純司, 柴田映子, 斯波真理子, 的場吉信, 土佐秀樹, 飯沼宗和	テネイシン抗体とα-マンゴスチンとの複合投与による乳癌転移抑制の試み	乳癌基礎研究	22	9-14	2013 (2014年度掲載)

Organic & Biomolecular Chemistry

PAPER

View Article Online
View Journal

Cite this: DOI: 10.1039/c5ob00242g

Amido-bridged nucleic acids with small hydrophobic residues enhance hepatic tropism of antisense oligonucleotides *in vivo*†

Tsuyoshi Yamamoto,‡[a,b] Aiko Yahara,‡[a] Reiko Waki,[a] Hidenori Yasuhara,[a,b] Fumito Wada,[a,b] Mariko Harada-Shiba[b] and Satoshi Obika*[a]

Received 4th February 2015,
Accepted 5th February 2015

DOI: 10.1039/c5ob00242g

www.rsc.org/obc

High scalability of a novel bicyclic nucleoside building block, amido-bridged nucleic acid (AmNA), to diversify pharmacokinetic properties of therapeutic antisense oligonucleotides is described. *N*2′-functionalization of AmNA with a variety of hydrophobic groups is straightforward. Combinations of these modules display similar antisense knockdown effects and improve cellular uptake, relative to sequence-matched conventional 2′,4′-bridged nucleic acid (2′,4′-BNA) *in vivo*.

Introduction

It has recently been demonstrated that naked therapeutic antisense oligonucleotides (AONs) exhibit robust systemic activity when comprised of several chemically modified nucleic acid building blocks.[1] In particular, conformationally constrained nucleotides such as 2′,4′-bridged nucleic acid (2′,4′-BNA) [also known as locked nucleic acid (LNA)][2] in combination with phosphorothioate (PS) exhibit extraordinarily high target RNA binding and acceptable pharmacokinetics. However, only a small fraction of the administered PS–LNAs is distributed in the target tissues;[3] most of the dose is deposited subcellularly, which is undesirable.[4] Thus, overcoming the pharmacokinetic challenges of AONs is necessary to improve their potency and to address safety concerns.[5]

A number of targeted delivery strategies for antisense therapeutics have been developed, including the terminal conjugation of biofunctional molecules.[6] However, these ligands often interfere with knockdown activity, despite their advantageous effect on the pharmacokinetics of AONs. In contrast, numerous LNA analogues with unique bridging structures have been developed and refined, and apparently minor structural modification of LNA can significantly alter their biological properties.[3a,7] However, the design and synthesis of this class of nucleotides are basically formidable. Therefore, evaluating the pharmacokinetics of AONs is formidable as well because we have only the option of evaluating them *in vivo*. On the other hand, Leumann *et al.* introduced hydrophobic side chains into the C6′-position of each tricyclo-DNA monomer through a metabolically labile ester group, then integrated these nucleotides into oligonucleotides and successfully improved cell-membrane permeability.[8] However, the effect of integration of these monomers on *in vivo* deposition remains obscure. In this context, we recently reported a promising alternative scaffold nucleoside, amido-bridged nucleic acid (AmNA),[9] which may be useful for addressing this issue (Fig. 1).

The furanose of AmNA is fused to a five-membered γ-lactam, whose amide bond is bridged between C2′ and C4′ of the ribose and rigidly fixed in C3′-*endo* conformation. The AmNA-modified AONs are much less susceptible to nuclease digestion than their LNA counterparts, possibly because of the steric hindrance of the *N*2′-methyl and neighboring carbonyl groups of the amide. These modified AONs maintain LNA-like high RNA affinity and show higher *in vitro* antisense activity than their LNA counterparts. Notably, *N*2′-functionalization is usually facile (AmNA[*N*-R]), making AmNA a promising building block for AONs. Other multivalent heteroatom-containing

[a]*Graduate School of Pharmaceutical Sciences, Osaka University, 1-6 Yamadaoka, Suita, Osaka 565-0871, Japan. E-mail: obika@phs.osaka-u.ac.jp; Fax: +81 6 6879 8204; Tel: +81 6 6879 8200*
[b]*Department of Molecular Innovation in Lipidology, National Cerebral and Cardiovascular Center Research Institute, 5-7-1 Fujishirodai, Suita, Osaka 565-8565, Japan*

†Electronic supplementary information (ESI) available. See DOI: 10.1039/c5ob00242g

‡These authors contributed equally to this work.

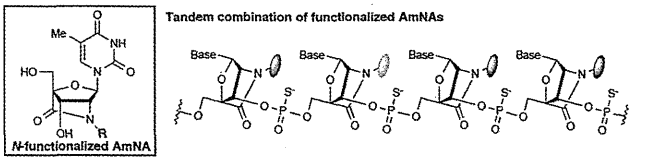

Fig. 1 Tandem arrangement strategy of *N*2′-functionalized AmNAs for improving the pharmacokinetics of antisense therapeutics.

BNAs, such as 2′-amino-LNA,[3c,10] 2′,4′-BNANC,[7f] *N*-Me-aminooxy BNA[7c] and 6′-thiol containing BNA,[11] are also intriguing alternatives in the same context, but *N*- or *S*-functionalized derivatives remain to be comprehensively developed.

To demonstrate the plasticity of our scaffold nucleoside for improving antisense therapeutics, we have developed a methodology to perturb the "*in vivo*" pharmacokinetics of AONs by using a variety of AmNA derivatives. Specifically, we synthesized AmNAs functionalized with a series of hydrophobic groups for potential improvement of intracellular and hepatic uptake of AONs and showed that hydrophobicity of the AmNA-AONs is readily adjustable by altering the substituents. We also demonstrated that a better tandem combination of *N*-alkylated AmNA (AmNA[*N*-R]) modules can improve hepatic disposition and potency of AONs *in vivo*.

Results and discussion

Phosphoramidite monomer synthesis

The phosphoramidite monomers corresponding to AmNA-[*N*-H] **4a** and AmNA[*N*-Me] **4b** were obtained as previously described.[9] From known nucleoside **1**, we synthesized the five monomers AmNA[*N*-Et] **4c**, AmNA[*N*-*n*Pr] **4d**, AmNA[*N*-iPr] **4e**, AmNA[*N*-Bn] **4f** and AmNA[*N*-Phen] **4g**, where abbreviated substituents indicate methyl, ethyl, *n*-propyl, i-propyl, benzyl and phenethyl, respectively (Scheme 1). Briefly, **1** was treated with sodium hydride, followed by the addition of the corresponding alkyl halides to give *N*-substituted compounds **2a–g**. Despite steric hindrance, these coupling reactions provided high yields under optimized conditions. Hydrogenolysis of the *O*3′, *O*5′-benzyl groups as well as *N*3-benzyloxymethyl groups of **2a–g** was effected using palladium on the carbon catalyst in THF followed by *O*5′-dimethoxytritylation to give *N*-substituted monomers **3a–g** in good yield over two steps (52–96%). Subsequent *O*3′-phosphitylation of **3a–g** was achieved with 2-cyanoethyl-*N*,*N*,*N*′,*N*′-tetraisopropylphosphorodiamidite to provide desired thymine phosphoramidites **4a–g**.

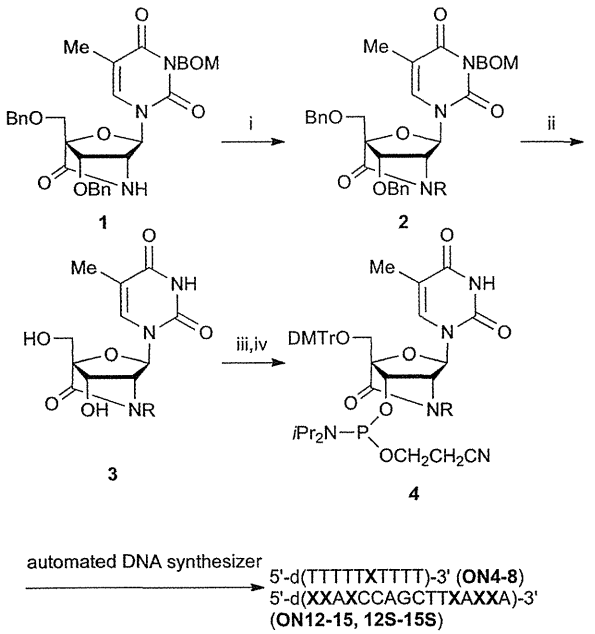

Scheme 1 Reagents and conditions: (i) NaH, RX, DMF, 0 °C → rt, R = Et: EtBr, quant.; R = *n*Pr: *n*PrBr, 76%; R = iPr: iPrI, quant.; R = Bn: BnBr, quant.; R = CH_2CH_2Ph: $BrCH_2CH_2Ph$, 43%; (ii) 20% $Pd(OH)_2/C$, H_2, THF, rt; (iii) DMTrCl, pyridine, rt, R = Et: 74% (2 steps); R = *n*Pr: 96% (2 steps); R = iPr: 81% (2 steps); R = Bn: 90% (2 steps); R = CH_2CH_2Ph: 83% (2 steps); (iv) $(i\text{-}Pr_2N)_2POCH_2CH_2CN$, *N*,*N*-diisopropylammonium tetrazolide, MeCN/THF (3 : 1), rt, R = Et: 77%; R = *n*Pr: 88%; R = iPr: 49%; R = Bn: 61%; R = CH_2CH_2Ph: 48%.

Oligonucleotide synthesis

Synthesis of oligonucleotides (ONs) containing AmNA[*N*-R] monomers was performed on an automated DNA synthesizer using a conventional phosphoramidite method. 5-[3,5-Bis(trifluoromethyl)phenyl]-1*H*-tetrazole (Activator 42®) solution was used for the synthesis of all the oligonucleotides described here. *N*-Alkylated AmNAs **4a–g** were successfully coupled using an extended coupling time to 16 min. The synthesized ONs were purified by reverse-phase HPLC (RP-HPLC) and the composition and purity were analyzed by MALDI-TOF mass spectrometry and RP-HPLC, respectively (Table 1 and ESI Table S1†). A purity greater than 95% was confirmed for all oligonucleotides. Note that the large-scale synthesis of phosphorothioate antisense oligonucleotides for *in vivo* usage and their purification were conducted by Gene Design Inc. (Ibaraki, Japan), where they used AmNA[*N*-R] phosphoramidite monomers provided by us and the composition and purity were analyzed by MALDI-TOF mass spectrometry and RP-HPLC, respectively.

Physicochemical properties of AmNA-containing oligonucleotides

We compared the relative hydrophobicity of oligonucleotides singly modified with AmNAs (**4a–g**; **ON-1–8**) by RP-HPLC using an octadecyl (C18) silica column under the indicated conditions. The obtained retention times are shown in Table 1. AmNA[*N*-H]-modified oligonucleotide **ON-2** was the most

Table 1 Oligonucleotides singly modified with AmNAs[a]

Oligonucleotides	ID	T_m (ΔT_m/mod.) (°C) RNA	DNA	Retention time (min)[b]
5′-d(TTTTTTTTTT)-3′	**ON-1**	19	21	8.4
5′-d(TTTTTt_HTTTT)-3′	**ON-2**	26 (+7)	20 (−1)	7.1
5′-d(TTTTTt_MTTTT)-3′	**ON-3**	26 (+7)	18 (−3)	10.7
5′-d(TTTTTt_ETTTT)-3′	**ON-4**	24 (+5)	18 (−3)	13.5
5′-d(TTTTTt_nTTTT)-3′	**ON-5**	21 (+2)	18 (−3)	15.5
5′-d(TTTTTt_iTTTT)-3′	**ON-6**	22 (+3)	17 (−4)	17.0
5′-d(TTTTTt_BTTTT)-3′	**ON-7**	23 (+4)	18 (−3)	22.4
5′-d(TTTTTt_PTTTT)-3′	**ON-8**	21 (+2)	18 (−3)	25.8

[a] t_H = AmNA[*N*-H], t_M = AmNA[*N*-Me], t_E = AmNA[*N*-Et] , t_n = AmNA[*N*-*n*Pr], t_i = AmNA[*N*-iPr], t_B = AmNA[*N*-Bn], and t_P = AmNA[*N*-Phen]. [b] Conditions: eluent A: 0.1 M TEAA buffer, eluent B: A/MeCN (1/1, v/v), gradient: MeCN conc. = 8–13% (30 min), 260 nm.

hydrophilic. As expected, the retention times of the derivatives varied as a function of the hydrophobicity of the oligonucleotides and could be adjusted by changing the substituents and their number.

To estimate the effect of modifications (**4a–g**) on duplex stability, the thermal stability of duplexes was measured with unmodified complementary RNA and DNA strands and compared with the melting temperatures of the corresponding unmodified reference duplexes (Table 1). Single incorporation of AmNAs **4a–g** into the center of a DNA T decamer increased thermal stability for complementary RNA (ΔT_m = +2 to +7 °C), but decreased stability for complementary DNA (ΔT_m = −1 to −4 °C), indicating that high RNA-selective binding is maintained. These results are consistent with previous observations made using a series of BNAs whose bridges differed in size and composition from LNA.[7a,12] A previous crystal structure study of DNA–LNA heteroduplex revealed that the 2′-oxygen of LNA forms hydrogen bonds with water molecules.[13] The perturbation of these hydration patterns by the 2′-substituents of AmNAs probably affected duplex stability, but all derivatives retained high affinity.

Nuclease stability

The effect of AmNA modification on nuclease resistance was determined by incorporating AmNAs into the second base from the 3′-end of oligonucleotides, followed by incubation with CAPV for 40 min at 37 °C. The percentage of intact oligonucleotides was analyzed by RP-HPLC and found to be higher than with conventional AmNA[*N*-Me] (ESI Fig. S5†).[7a]

In vivo activities of AmNA-modified antisense oligonucleotides

We next evaluated hydrophobic AmNA-modified AONs *in vivo*. We previously developed a potent LNA-based AON that targets apolipoprotein CIII (apoC-III) for the treatment of dyslipidemia.[14] Truncated versions of this apoC-III AON were used in these *in vivo* studies because we recently revealed that these could be more potent.[3d,15] Six LNAs were incorporated into a 16-mer PS-AON, **ON-9S**. **ON-10S** retains a seven natural-nucleotide gap moiety, sufficient for maintaining RNase H (a key enzyme for antisense mechanism)-recruiting activity.

The primary purpose of the *in vivo* study was to confirm the effectiveness of this truncated version of LNA-AON to target apoC-III mRNA, and mice were dosed intravenously with **ON-10S** at a dose range of 5–20 mg kg^{-1}. The expression levels of apoC-III mRNA in the liver were analysed 72 hours post-injection. Dose-dependent reduction in hepatic apoC-III mRNA through a single administration of **ON-10S** was observed without significant toxicity (ESI Fig. S6, S7.† The highest reduction in hepatic apoC-III mRNA (60%) was recorded at a dose of 20 mg kg^{-1}, and statistical significance with saline control was found at doses above 10 mg kg^{-1}. Thus, hydrophobic AmNAs-carrying AONs were evaluated *in vivo* at 15 mg kg^{-1}.

N-Alkylated AmNAs **4b, e, f** were introduced into PS-AON **ON-9S** to obtain **ON-11S** to **-13S** as shown in Table 2. The relative hydrophobicity of the oligonucleotides was gauged from their elution time of RP-HPLC.

Table 2 Antisense oligonucleotides targeting murine apoC-III mRNA[a]

Oligonucleotides	ID	T_m (ΔT_m/mod.) (°C) RNA	Retention time (min)[b]
5′-d(TTATCCAGCTTTATTA)-3′	**ON-9S**	39	5.8
5′-d($t_Lt_LAt_LCCAGCTTt_LAt_Lt_LA$)-3′	**ON-10S**	63 (+4)	5.8
5′-d($t_Mt_MAt_MCCAGCTTt_MAt_Mt_MA$)-3′	**ON-11S**	63 (+4)	5.8
5′-d($t_it_iAt_iCCAGCTTt_iAt_it_iA$)-3′	**ON-12S**	61 (+4)	10.6
5′-d($t_Bt_BAt_BCCAGCTTt_BAt_Bt_BA$)-3′	**ON-13S**	59 (+3)	21.2
5′-d($t_it_iAt_MCCAGCTTt_MAt_it_iA$)-3′	**ON-14S**	62 (+4)	11.0
5′-d($t_Bt_MAt_MCCAGCTTt_MAt_Mt_BA$)-3′	**ON-15S**	63 (+4)	13.0

[a] t_L = LNA-T, t_M = AmNA[*N*-Me], t_i = AmNA[*N*-iPr] and t_B = AmNA[*N*-Bn]. [b] Conditions: eluent A: 0.1 M TEAA buffer, eluent B: A/MeCN (1/1, v/v), gradient: MeCN conc. = 13–37% (30 min), 260 nm.

Each PS modification increases the retention time of the AON; consequently the content of acetonitrile in the elution buffer was modified from 8–13% to 13–37%, as described in the footnote to Table 2. The retention times for **ON-11S** to **-13S** differed significantly and predictably from the singly-incorporated phosphodiester-version oligonucleotides (**ON-3, -6, -7**; Table 1). AmNA[*N*-Bn] **4f** and AmNA[*N*-^{i}Pr] **4e** increased the hydrophobicity of the AON, whereas steric hindrance of the gap moiety in **ON-12S** and **-13S** reduced potency. Therefore, we further designed and synthesized **ON-14S** and **-15S**, which showed well-controlled retention times. The T_m values of **ON-11S** to **-15S** were measured and found to be in approximately 60 °C under the indicated buffer conditions. C57Bl/6J male mice (n = 3 per group) were intravenously injected with **ON-10S, -11S, -12S, -13S, -14S** or **-15S** at a dose of 2.9 μmol kg^{-1} (15 mg kg^{-1} for **ON-10S**). LNA counterpart **ON-10S** reduced apoC-III by 45%, and AmNA-AONs **ON-11S** and **ON-12S** achieved a similar knockdown of 40% and 30% respectively. This is the first demonstration of AmNA-AONs exhibiting LNA congener-like high activity *in vivo* (Fig. 2, ESI Fig. S8†). In contrast, AmNA[*N*-Bn] **4f**-based AON **ON-13S** showed no knockdown. The less hindered **ON-14S** and **-15S** in the gaps showed improved potency compared to **-11S, -12S**; interestingly, **ON-14S** achieved the highest knockdown of apoC-III mRNA of the AmNA-AONs tested, suggesting that a combination of functionalized AmNAs working in tandem can tailor potency of AONs.

Hepatic tropism of hydrophobic AmNA-modified antisense oligonucleotides

To investigate whether different combinations of hydrophobic AmNAs alter the tissue deposition of AONs, we measured the intact AONs that accumulated in the liver after intravenous administration using a previously described ELISA method.[16] The hepatic distribution of the more hydrophobic **ON-12S, -13S, -14S** and **-15S** was ~1.5 times higher than that of the LNA-AON **ON-10S**, whereas **ON-10S** and **ON-11S** exhibited

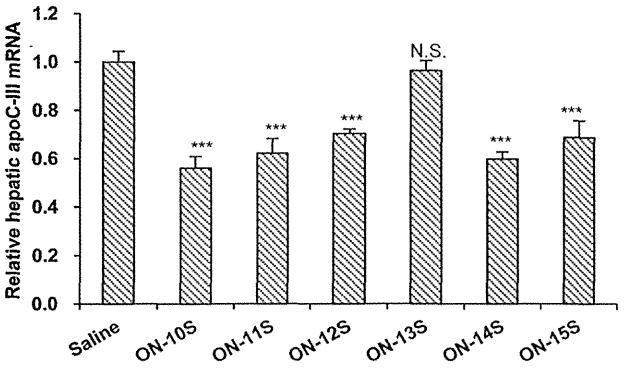

Fig. 2 Reduction of apoC-III mRNA in the livers of mice receiving a single intravenous dose of 2.868 μmol kg^{-1} of a series of AONs. Dunnett's multiple comparison test, ***$P < 0.001$, N.S.; not significant. Error bars represent group means + S.D. $n = 3$.

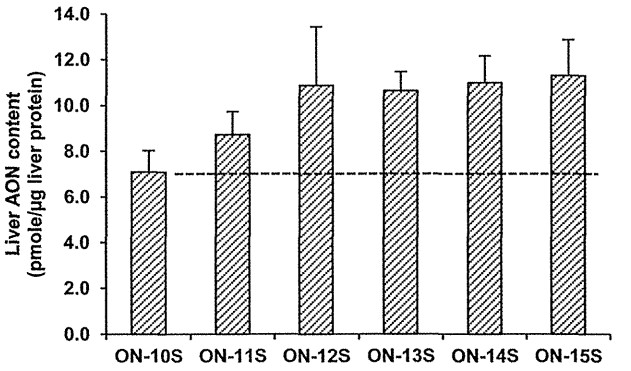

Fig. 3 ELISA-based quantification of a series of AONs distributed in murine liver after 72 hours post-injection. Error bars represent group means + S.D. $n = 3$.

hepatic distribution similar to each other (Fig. 3). However, the activity of all these AmNA-based AONs was at best comparable to the LNA counterpart **ON-10S**. It should primarily be noted that no statistical significance was found between these liver AON contents, which may contribute to this insignificant change in potency. It is also possible that the hydrophobic modification altered the suborgan distribution of AONs in liver. ApoC-III mRNA is predominantly expressed in hepatic parenchymal cells, which comprise 80% of the liver volume, whereas non-parenchymal cells such as Kupffer cells and sinusoidal endothelial cells are relatively minor components of the liver. AONs should therefore selectively target the parenchymal cells. However, it is reported that 80% of PS-AONs accumulated in the liver are distributed in non-parenchymal cells and only 20% are in the parenchymal hepatocytes.[4b] The hydrophobic AONs developed here might foster this trend. Alternatively, there are at least two uptake pathways in parenchymal cells (a productive pathway and a bulk nonproductive pathway); the hydrophobic AONs might encourage the nonproductive uptake which undermines the knockdown activity of AONs.[4a]

Conclusions

In summary, we here showed that AmNAs are an interesting class of antisense building blocks. A series of AmNAs functionalized with a variety of hydrophobic groups were synthesized: AmNA[*N*-Et] **4c**, AmNA[*N*-*n*Pr] **4d**, AmNA[*N*-iPr] **4e**, AmNA-[*N*-Bn] **4f** and AmNA[*N*-Phen] **4g**. We demonstrated that a tandem arrangement of these small substituents affects the systemic activity and tissue disposition of AONs *in vivo*. This strategy will allow more finely-tuned control of the properties of AONs than conventional strategies. Using this scaffold nucleoside, we will further develop useful modules and identify the best combination of these AmNA modules to tackle the issues currently confronting antisense therapeutics.

Experimental

General

All moisture-sensitive reactions were carried out in well-dried glassware under a N_2 atmosphere. Anhydrous dichloromethane, DMF, MeCN, and pyridine were used as purchased. ^{1}H NMR spectra were recorded at 300 and 400 MHz and 500 MHz, ^{13}C NMR were recorded at 75 and 100 MHz, and the ^{31}P spectrum was recorded at 161 MHz. Chemical shift values are expressed in δ values (ppm) relative to tetramethylsilane (TMS) as an internal standard and a residual solvent for ^{1}H NMR, and $CHCl_3$ (δ = 77.00 ppm), methanol (δ = 49.00 ppm), and DMSO (39.50 ppm) for ^{13}C NMR, and 85% H_3PO_4 (δ = 0 ppm) for ^{31}P NMR. Fast atom bombardment mass spectra (FAB-MS) were recorded in the positive ion mode. For column chromatography, silica gel PSQ 100B was used. Progress of the reaction was monitored by analytical thin layer chromatography (TLC) on pre-coated aluminium sheets (Silica gel 60 F_{254} sheet, Merck), and the products were visualized by UV light.

Synthesis of AmNA monomers and phosphoramidites

General procedure 1 (synthesis of compound 2). To the stirring solution of **1** (1.0 equiv.) in DMF (0.1 M) was added NaH (1.2 equiv.) at 0 °C. After stirring for 30 min, alkyl halide (1.2 equiv.) was added. The reaction temperature was gradually raised from 0 °C to room temperature and after completion of the reaction (approx. 30 min), ice-cold water was added. The solution was stirred for 15 min and the product was extracted with ethyl acetate. The organic phase was washed with brine, dried (Na_2SO_4), and concentrated. The product was purified by flash column chromatography (*n*-hexane–ethyl acetate = 3 : 1 or 2 : 1) to afford **2** as a white amorphous solid.

*(2'R)-3',5'-Di-O-benzyl-N^3-benzyloxymethyl-2'-ethylamino-2'-N,4'-C-oxomethylenethymidine (**2c**: R = Et).* By following the general procedure 1, using bromoethane as an alkyl halide, **2c** was obtained in quant. as a white amorphous solid.

$[\alpha]_D^{23}$ +45.9 (*c* 0.100, $CHCl_3$). IR (KBr): 3071, 3033, 2930, 2871, 1725, 1708, 1665, 1454, 1273 cm^{-1}. ^{1}H NMR (300 MHz, $CDCl_3$) δ: 1.22 (3H, t), 1.64 (3H, s), 3.35 (1H, dq J = 14 Hz,

7 Hz), 3.52 (1H, dq J = 14 Hz, 7 Hz), 3.95, 4.10 (2H, AB, J = 11.5 Hz), 4.07 (1H, s), 4.13 (1H, s), 4.52, 4.54 (2H, AB, J = 12 Hz), 4.59, 4.63 (2H, AB, J = 11.5 Hz), 4.70 (2H, s), 5.39 (1H, s), 5.45, 5.47 (2H, AB, J = 9.5 Hz), 7.18–7.39 (15H, m), 7.54 (1H, s). ^{13}C NMR (100 MHz, $CDCl_3$) δ: 12.8, 13.7, 36.5, 62.4, 63.2, 70.1, 72.2, 72.3, 73.7, 76.7, 78.1, 85.4, 87.6, 109.8, 127.6, 127.6, 127.9, 128.1, 128.4, 133.8, 136.3, 137.4, 137.6, 150.5, 163.1, 170.1. MS (FAB): m/z 612 $[M + H]^+$. HRMS (FAB): calcd for $C_{35}H_{38}N_3O_7$ $[M + H]^+$: 612.2710. Found: 612.2693.

*(2'R)-3',5'-Di-O-benzyl-N^3-benzyloxymethyl-2'-propylamino-2'-N,4'-C-oxomethylenethymidine (**2d**: R = nPr).* By following the general procedure 1, using 1-bromopropane as an alkyl halide, **2d** was obtained in 76% as a white amorphous solid.

$[\alpha]_D^{23}$ +29.2 (c 1.000, $CHCl_3$). IR (KBr): 3066, 3029, 2910, 2863, 1724, 1709, 1664, 1455, 1274 cm^{-1}. ^{1}H NMR (300 MHz, $CDCl_3$) δ: 0.93 (3H, q, J = 7.0 Hz), 1.56–1.64 (2H, m), 1.64 (3H, s), 3.33 (2H, ddq), 3.95, 4.09 (2H, AB, J = 12 Hz), 4.07 (1H, s), 4.13 (1H, s), 4.53 (2H, s), 4.59, 4.65 (2H, AB, J = 11.0 Hz), 4.71 (2H, s), 5.40 (1H, s), 5.46 (2H, t, J = 9.5 Hz), 7.19–7.37 (15H, m), 7.54 (1H, s). ^{13}C NMR (100 MHz, $CDCl_3$) δ: 11.1, 12.9, 21.9, 43.4, 62.9, 63.3, 70.2, 72.3, 72.3, 72.4, 73.8, 78.2, 85.3, 87.5, 109.8, 127.6, 127.6, 127.6, 127.7, 128.0, 128.2, 128.2, 128.2, 128.4, 133.8, 136.3, 137.4, 137.4, 137.7, 150.6, 163.2, 170.5. MS (FAB): m/z 626 $[M + H]^+$. HRMS (FAB): calcd for $C_{36}H_{40}N_3O_7$ $[M + H]^+$: 626.2866. Found: 626.2867.

*(2'R)-3',5'-Di-O-benzyl-N^3-benzyloxymethyl-2'-isopropylamino-2'-N,4'-C-oxomethylenethymidine (**2e**: R = iPr).* By following the general procedure 1, using 2-iodopropane as an alkyl halide, **2e** was obtained in quant. as a white amorphous solid.

$[\alpha]_D^{23}$ +57.2 (c 1.000, $CHCl_3$). IR (KBr): 3064, 3031, 2927, 2873, 1728, 1708, 1666, 1455, 1275 cm^{-1}. ^{1}H NMR (400 MHz, $CDCl_3$) δ: 1.18 (3H, d, J = 7 Hz), 1.31 (3H, d, J = 7 Hz), 1.64 (3H, s), 3.94, 4.10 (2H, AB, J = 12 Hz), 4.07 (1H, s), 4.28 (1H, s), 4.36–4.47 (1H, m), 4.50, 4.54 (2H, AB, J = 11.5 Hz), 4.58, 4.63 (2H, AB, J = 11.5 Hz), 4.71 (2H, s), 5.37 (1H, s), 5.46, 5.49 (2H, AB, J = 9.5 Hz), 7.18–7.39 (15H, m), 7.54 (1H, s). ^{13}C NMR (100.53 MHz, $CDCl_3$) δ: 12.9, 20.6, 21.1, 42.6, 58.9, 63.2, 70.1, 72.2, 72.2, 73.7, 78.2, 86.1, 88.0, 109.6, 127.3, 127.4, 127.5, 127.6, 127.6, 127.9, 128.1, 128.2, 128.2, 128.4, 129.4, 133.8, 136.2, 137.4, 137.7, 150.5, 163.2, 169.4. MS (FAB): m/z 626 $[M + H]^+$. HRMS (FAB): calcd for $C_{36}H_{40}N_3O_7$ $[M + H]^+$: 626.2866. Found: 626.2869.

*(2'R)-3',5'-Di-O-benzyl-N^3-benzyloxymethyl-2'-benzylamino-2'-N,4'-C-oxomethylenethymidine (**2f**: R = Bn).* By following the general procedure 1, using bromomethylbenzene as an alkyl halide, **2f** was obtained in quant. as a white amorphous solid.

$[\alpha]_D^{23}$ +17.1 (c 1.000, $CHCl_3$). IR (KBr): 3064, 3030, 2871, 1728, 1665, 1454, 1277 cm^{-1}. ^{1}H NMR (300 MHz, $CDCl_3$) δ: 1.60 (3H, s), 3.98, 4.12 (2H, AB, J = 12 Hz), 4.20, 4.26 (2H, AB, J = 11 Hz), 4.21, 4.85 (2H, AB, J = 15 Hz), 4.58, 4.65 (2H, AB, J = 11.5 Hz), 4.67 (2H, s), 5.34 (1H, s), 5.39, 5.45 (2H, AB, J = 9.5 Hz), 7.02–7.36 (20H, m), 7.48 (2H, s). ^{13}C NMR (100 MHz, $CDCl_3$) δ: 13.0, 45.1, 61.9, 63.2, 70.3, 72.3, 72.4, 74.0, 77.8, 85.0, 87.5, 109.9, 127.5, 127.7, 127.8, 128.0, 128.1, 128.1, 128.3, 128.4, 128.6, 128.6, 128.8, 133.9, 135.8, 136.2, 137.5, 137.8, 140.0, 150.5, 151.6, 163.3, 170.5. MS (FAB): m/z 674 $[M + H]^+$. HRMS (FAB): calcd for $C_{40}H_{40}N_3O_7$ $[M + H]^+$: 674.2866. Found: 674.2841.

*(2'R)-3',5'-Di-O-benzyl-N^3-benzyloxymethyl-2'-phenethylamino-2'-N,4'-C-oxomethylenethymidine (**2g**: R = CH_2CH_2Ph).* By following the general procedure 1, using 2-bromoethylbenzene as an alkyl halide, **2g** was obtained in 43% as a white amorphous solid.

$[\alpha]_D^{24}$ +0.2 (c 0.320, $CHCl_3$). IR (KBr): 3029, 2930, 1722, 1701, 1667, 1453, 1274 cm^{-1}. ^{1}H NMR (300 MHz, $CDCl_3$) δ: 1.62 (3H, s), 2.82–3.02 (2H, m), 3.52–3.75 (2H, m), 3.94, 4.08 (2H, AB, J = 12 Hz), 4.02 (1H, s), 4.12 (1H, s), 4.44 (2H, s), 4.58, 4.63 (2H, AB, J = 11.5 Hz), 4.70 (2H, s), 5.29 (1H, s), 5.44, 5.48 (2H, AB, J = 9.5 Hz), 7.14–7.40 (20H, m), 7.49 (1H, s). ^{13}C NMR (100.53 MHz, $CDCl_3$) δ: 13.0, 34.7, 43.1, 63.3, 63.3, 70.3, 72.4, 72.5, 74.0, 78.3, 85.3, 87.5, 110.0, 126.7, 127.7, 127.7, 127.8, 128.1, 128.3, 128.3, 128.6, 128.6, 128.7, 133.9, 136.4, 137.5, 137.8, 137.9, 150.6, 163.3, 170.7. MS (FAB): m/z 688 $[M + H]^+$. HRMS (FAB): calcd for $C_{41}H_{42}N_3O_7$ $[M + H]^+$: 688.3023. Found: 688.3015.

General procedure 2 (synthesis of compound 3). To the solution of **2** (1.0 equiv.) in THF or methanol (0.1 M) was added 20% palladium on carbon (1.0 w/w) and the reaction vessel was degassed several times with hydrogen. The reaction mixture was stirred under a hydrogen atmosphere for 1–5 h at room temperature. After completion of the reaction, the reaction solution was filtered using filter paper and washed thoroughly with hot methanol. After evaporation of solvents, the product was dissolved with methanol (0.3 M) and 28% ammonia solution (0.3 M) was added and the solution was stirred at room temperature. After 5 min, the product was concentrated to afford **S1** as a white solid.

To the solution of **S1** in anhydrous pyridine (0.1 M) was added DMTrCl (1.3 equiv.) and the solution was stirred at room temperature. After stirring for 1–19 h, ice-cold water was added and the product was extracted with ethyl acetate. The organic phase was washed with brine, dried (Na_2SO_4), and concentrated. The product was purified by flash column chromatography (n-hexane–ethyl acetate = 1 : 1 or 1 : 3) to afford **3** as a white amorphous solid.

*(2'R)-5'-O-(4,4'-Dimethoxytrityl)-2'-ethylamino-2'-N,4'-C-oxomethylenethymidine (**3c**: R = Et).* By following the general procedure 2, **3c** was obtained in 45% (for 2 steps) as a white amorphous solid.

$[\alpha]_D^{25}$ +12.9 (c 1.000, $CHCl_3$). IR (KBr): 3087, 2967, 2872, 1729, 1698, 1665, 1509, 1464 cm^{-1}. ^{1}H NMR (300 MHz, $CDCl_3$) δ: 1.16 (3H, t, J = 7 Hz), 1.62 (3H, s), 3.23–3.55 (2H, m), 3.63, 3.84 (2H, AB, J = 11.5 Hz), 3.74 (6H, s), 4.10 (1H, s), 4.24 (1H, s), 4.51 (1H, s), 5.39 (1H, s), 6.79–6.83 (4H, m), 7.13–7.45 (9H, m), 7.81 (1H, s), 10.33 (1H, s). ^{13}C NMR (100.53 MHz, $CDCl_3$) δ: 12.4, 13.4, 36.5, 55.1, 56.3, 64.9, 72.6, 85.3, 86.6, 88.8, 110.5, 112.9, 113.2, 127.0, 127.6, 127.8, 127.9, 129.0, 130.0, 135.1, 135.4, 144.3, 150.2, 158.4, 164.6, 170.5. MS (FAB): m/z 636 $[M + Na]^+$. HRMS (FAB): calcd for $C_{34}H_{35}N_3O_8Na$ $[M + Na]^+$: 636.2322. Found: 636.2312.

*(2'R)-5'-O-(4,4'-Dimethoxytrityl)-2'-propylamino-2'-N,4'-C-oxomethylenethymidine (**3d**: R = nPr).* By following the general

procedure 2, **3d** was obtained in 96% (for 2 steps) as a white amorphous solid.

$[\alpha]_D^{26}$ +33.1 (*c* 1.000, $CHCl_3$). IR (KBr): 3384, 3021, 2838, 1704, 1699, 1509, 1254 cm^{-1}. ^1H NMR (300 MHz, $CDCl_3$) δ: 1.17 (3H, t, J = 7 Hz), 1.62 (3H, s), 3.34–3.58 (2H, m), 3.61, 3.90 (2H, AB, J = 12 Hz), 3.91–3.98 (2H, m), 3.88 (6H, s), 4.28 (1H, s), 4.53 (1H, d, J = 7 Hz), 5.50 (1H, s), 6.83–6.85 (4H, m), 7.23–7.36 (7H, m), 7.44 (2H, d, J = 7 Hz), 7.82 (1H, s), 9.40 (1H, s). ^{13}C NMR (75 MHz, $CDCl_3$) δ: 11.2, 12.5, 21.7, 43.6, 55.2, 56.5, 65.2, 72.8, 85.2, 86.9, 88.6, 110.7, 113.3, 113.4, 127.1, 127.9, 128.1, 130.0, 135.1, 135.3, 144.3, 150.1, 158.6, 164.3, 170.6. MS (FAB): *m/z* 650 $[M + Na]^+$. HRMS (FAB): calcd for $C_{35}H_{37}N_3O_8Na$ $[M + Na]^+$: 650.2478. Found: 650.2508.

*(2'R)-5'-O-(4,4'-Dimethoxytrityl)-2'-isopropylamino-2'-N,4'-C-oxomethylenethymidine (**3e**: R = iPr).* By following the general procedure 2, **3e** was obtained in 78% (for 2 steps) as a white amorphous solid.

$[\alpha]_D^{23}$ −3.83 (*c* 1.000, $CHCl_3$). IR (KBr): 3366, 3190, 2968, 2836, 1704, 1686, 1509, 1249 cm^{-1}. ^1H NMR (300 MHz, $CDCl_3$) δ: 1.17 (3H, d, J = 6.5 Hz), 1.28 (3H, d, J = 6.5 Hz), 1.69 (3H, s), 2.54 (1H, s), 3.59, 3.92 (2H, AB, J = 12 Hz), 3.77 (6H, s), 4.28 (1H, s), 4.28–4.37 (1H, m), 4.40 (1H, s), 5.37 (1H, s), 6.82–6.84 (4H, m), 7.20–7.36 (7H, m), 7.44 (2H, d, J = 7 Hz), 7.79 (1H, s), 9.65 (1H, s). ^{13}C NMR (100.53 MHz, $CDCl_3$): δ 12.5, 20.5, 21.1, 42.8, 55.2, 56.5, 61.5, 72.9, 86.0, 86.9, 89.2, 110.6, 113.3, 113.4, 127.1, 127.9, 128.1, 130.0, 135.2, 135.3, 144.4, 150.1, 158.6, 164.3, 169.4. MS (FAB): *m/z* 650 $[M + Na]^+$. HRMS (FAB): calcd for $C_{35}H_{37}N_3O_8Na$ $[M + Na]^+$: 650.2478. Found: 650.2490.

*(2'R)-5'-O-(4,4'-Dimethoxytrityl)-2'-benzylamino-2'-N,4'-C-oxomethylenethymidine (**3f**: R = Bn).* By following the general procedure 2, **3f** was obtained in 90% (for 2 steps) as a white amorphous solid.

$[\alpha]_D^{25}$ +3.8 (*c* 1.000, $CHCl_3$). IR (KBr): 3063, 2967, 2837, 1686, 1607, 1509, 1249 cm^{-1}. ^1H NMR (300 MHz, $CDCl_3$) δ: 1.57 (3H, s), 3.67, 3.88 (2H, AB, J = 12 Hz), 3.74 (6H, s), 4.21 (1H, s), 4.44 (1H, s), 4.47, 4.52 (2H, AB, J = 15 Hz), 5.13 (1H, s), 6.79–6.83 (4H, m), 7.14–7.34 (7H, m), 7.39–7.44 (2H, d, J = 7 Hz), 7.74 (1H, s), 9.97 (1H, s). ^{13}C NMR (75 MHz, $CDCl_3$): δ 12.5, 45.6, 55.2, 56.5, 65.1, 72.4, 84.7, 86.8, 88.7, 110.6, 113.0, 113.3, 127.1, 127.9, 128.0, 128.7, 128.8, 130.0, 135.1, 135.2, 135.7, 144.3, 150.1, 158.6, 164.4, 170.7. MS (FAB): *m/z* 698 $[M + Na]^+$. HRMS (FAB): calcd for $C_{39}H_{37}N_3O_8Na$ $[M + Na]^+$: 698.2478. Found: 698.2484.

*(2'R)-5'-O-(4,4'-Dimethoxytrityl)-2'-phenethyl amino-2'-N,4'-C-oxomethylenethymidine (**3g**: R = CH_2CH_2Ph).* By following the general procedure 2, **3g** was obtained in 84% (for 2 steps) as a white amorphous solid.

$[\alpha]_D^{21}$ +4.6 (*c* 0.400, $CHCl_3$). IR (KBr): 3190, 2958, 2929, 1721, 1694, 1672, 1509, 1270 cm^{-1}. ^1H NMR (300 MHz, $CDCl_3$) δ: 1.67 (3H, d, J = 8.5 Hz), 2.93–3.01 (2H, m), 3.56–3.66 (1H, m), 3.58, 3.87 (2H, AB, J = 12 Hz), 3.81 (7H, m), 4.07 (1H, s), 4.22 (1H, m), 4.34 (1H, s), 5.30 (1H, s), 6.83–7.85 (4H, m), 7.16–7.54 (14H, m), 7.72 (1H, d, J = 8.5 Hz), 8.61 (1H, s). ^{13}C NMR (75 MHz, $CDCl_3$) δ: 13.0, 34.7, 43.1, 63.3, 63.3, 70.3, 72.4, 72.5, 74.0, 78.3, 85.3, 87.5, 109.9, 126.7, 127.7, 127.7, 127.8, 128.1, 128.3, 128.3, 128.6, 128.6, 128.7, 133.9, 136.4, 137.5, 137.8, 137.9, 150.6, 163.3, 170.7. MS (FAB): *m/z* 712 $[M + Na]^+$. HRMS (FAB): calcd for $C_{40}H_{39}N_3O_8Na$ $[M + Na]^+$: 712.2635. Found: 712.2631.

General procedure 3 (synthesis of compound 4). To the solution of 3 (1.0 equiv.) in anhydrous MeCN–THF (3 : 1, 0.1 M) were added *N,N*-diisopropylammonium tetrazolide (0.75 equiv.) and 2-cyanoethyl-*N,N,N′,N′*-tetraisopropylphosphorodiamidite (1.2 equiv.). After stirring at room temperature for 9 h–19 h, ice-cold water was added and the product was extracted with ethyl acetate. The organic phase was washed with brine, dried (Na_2SO_4), and concentrated. The product was purified by flash column chromatography (0.05 eq. of triethylamine in *n*-hexane–ethyl acetate = 1 : 1) to afford **4c** (R = Et: 39 mg, 77%) as a white amorphous solid.

*(2'R)-3'-O-[2-Cyanoethoxy(disopropylamino)phosphino]-5'-O-(4,4'-dimethoxytrityl)-2'-ethylamino-2'-N,4'-C-oxomethylenethymidine (**4c**: R = Et).* By following the general procedure 3, **4c** was obtained in 77% as a white amorphous solid.

M.p. 100–103 °C (CH_2Cl_2–hexane). ^{31}P NMR (161.83 MHz, $CDCl_3$) δ: 149.2, 150.3. MS (FAB): *m/z* 814 $[M + H]^+$. HRMS (FAB): calcd for $C_{43}H_{53}N_5O_9P$ $[M + H]^+$: 814.3581. Found: 814.3588.

*(2'R)-3'-O-[2-Cyanoethoxy(disopropylamino)phosphino]-5'-O-(4,4'-dimethoxytrityl)-2'-propylamino-2'-N,4'-C-oxomethylenethymidine (**4d**: R = nPr).* By following the general procedure 3, **4d** was obtained in 88% as a white amorphous solid.

M.p. 83–86 °C (CH_2Cl_2–hexane). ^{31}P NMR (161.83 MHz, $CDCl_3$) δ: 149.8, 150.2. MS (FAB): *m/z* 828 $[M + H]^+$. HRMS (FAB): calcd for $C_{44}H_{55}N_5O_9P$ $[M + H]^+$: 828.3737. Found: 828.3745.

*(2'R)-3'-O-[2-Cyanoethoxy(disopropylamino)phosphino]-5'-O-(4,4'-dimethoxytrityl)-2'-isopropylamino-2'-N,4'-C-oxomethylenethymidine (**4e**: R = iPr).* By following the general procedure 3, **4e** was obtained in 32% as a white amorphous solid.

M.p. 101–104 °C (CH_2Cl_2–hexane). ^{31}P NMR (161.83 MHz, $CDCl_3$) δ: 149.5, 151.3. MS (FAB): *m/z* 828 $[M + H]^+$. HRMS (FAB): calcd for $C_{44}H_{55}N_5O_9P$ $[M + H]^+$: 828.3737. Found: 828.3729.

*(2'R)-3'-O-[2-Cyanoethoxy(disopropylamino)phosphino]-5'-O-(4,4'-dimethoxytrityl)-2'-benzylamino-2'-N,4'-C-oxomethylenethymidine (**4f**: R = Bn).* By following the general procedure 3, **4f** was obtained in 61% as a white amorphous solid.

M.p. 99–101 °C (CH_2Cl_2–hexane). ^{31}P NMR (161.83 MHz, $CDCl_3$) δ: 150.0, 150.2. MS (FAB): *m/z* 876 $[M + H]^+$. HRMS (FAB): calcd for $C_{48}H_{55}N_5O_9P$ $[M + H]^+$: 876.3737. Found: 876.3735.

*(2'R)-3'-O-[2-Cyanoethoxy(disopropylamino)phosphino]-5'-O-(4,4'-dimethoxytrityl)-2'-phenethylamino-2'-N,4'-C-oxomethylenethymidine (**4g**: R = CH_2CH_2Ph).* By following the general procedure 3, **4g** was obtained in 48% as a white amorphous solid.

M.p. 98–101 °C (CH_2Cl_2–hexane). ^{31}P NMR (161.83 MHz, $CDCl_3$) δ: 149.6, 150.8. MS (FAB): *m/z* 890 $[M + H]^+$. HRMS (FAB): calcd for $C_{49}H_{57}N_5O_9P$ $[M + H]^+$: 890.3894. Found: 890.3909.

Synthesis, purification and characterization of oligonucleotides

Synthesis of 0.2 μmol scale of oligonucleotides **ON-6-44** modified with AmNA[*N*-Me] was performed using Oligonucleotide Synthesizer (Gene Design, ns-8) according to the standard phosphoramidite protocol with Activator 42™ (Proligo) as the activator. Dry MeCN was used to dissolve AmNA[*N*-R]. The standard synthesis cycle was used for assembly of the reagents and synthesis of the oligonucleotides, except that the coupling time was extended to 16 minutes for AmNA[*N*-R] monomers. (The coupling time for AmNA[*N*-Me] was 32 seconds.) The synthesis was carried out in trityl on mode and was treated with concentrated ammonium hydroxide at room temperature for 1 h to cleave the synthesized oligonucleotides from the solid support. The oligonucleotides were initially purified by Sep-pack Plus C_{18} Environmental Cartridge. The separated oligonucleotides were further purified by reverse-phase HPLC with Waters Xbridge™ Shield RP_{18} 2.5 μm (10 mm × 50 mm) columns with a linear gradient of MeCN (7–13% over 42 min for **ON-3–6, ON-11, ON-12, ON-16**, 8–15% over 42 min for **ON-7, ON-8**, 13–40% over 42 min for **ON-13, ON-17**) in 0.1 M triethylammonium acetate (pH 7.0). The oligonucleotides were analyzed for purity by HPLC and characterized by MALDI-TOF mass spectroscopy.

UV melting experiments and melting profiles

The UV melting experiments were carried out using a Shimadzu UV-1650 spectrometer equipped with a T_m analysis accessory. Equimolecular amounts of the target RNA or DNA strand and oligonucleotide were dissolved in buffer A (10 mM phosphate buffer at pH 7.2 containing 100 mM NaCl) to give a final strand concentration of 4 μM. The samples were annealed by heating at 95 °C followed by slow cooling to room temperature. The melting profile was recorded at 260 nm from 0 to 70 °C (for **ON-3–8**), from 5 to 100 °C (for **ON-11–13, 16, 17**) at a scan rate of 0.5 °C min^{-1}. The T_m was calculated as the temperature of the half-dissociation of the formed duplexes, determined by the midline of the melting curve.

Enzymatic digestion study

The sample solutions were prepared by dissolving 0.75 μmol of oligonucleotides in 50 mM Tris-HCl buffer (pH 8.0) containing 10 mM $MgCl_2$. To each sample solution, 0.175 μL *Crotalus adamanteus* venom phosphodiesterase (CAVP) was added and the cleavage reaction was carried out at 37 °C. A portion of each reaction mixture was removed at timed intervals and heated to 90 °C for 5 min to deactivate the nuclease. Aliquots of the timed samples were analyzed by RP-HPLC to evaluate the amount of intact oligonucleotides remaining. The percentage of intact oligonucleotide in each sample was calculated and plotted against the digestion time to obtain a degradation curve with time (Fig. S5†).

In vivo knockdown study

All animal procedures were performed in accordance with the guidelines of the Animal Care Ethics Committee of the National Cerebral and Cardiovascular Center Research Institute (Osaka, Japan). All animal studies were approved by an Institutional Review Board. C57BL/6J mice were obtained from CLEA Japan. All mice were male, and studies were initiated when animals were 8 weeks of age. Mice (n = 3 per arm) were maintained on a 12 h light/12 h dark cycle and fed *ad libitum*. Mice were fed a normal chow (CE-2, CLEA Japan) for 2 weeks before and during treatment. Mice received single treatment of saline-formulated AONs intravenously. At the time of sacrifice after 72 hours of injection, mice were subjected to blood collection from tail veins and then anesthetized with isoflurane (Forane, Abbott Japan) under an overnight fasting condition. Livers were harvested and snap frozen until subsequent analysis. Whole blood was collected and subjected to serum separation for subsequent analysis.

mRNA quantification

Frozen liver tissue was collected in a 2 mL tube with 1 mL of TRIzol Reagent (Life Technologies, Japan) and a zirconia ball (Ø 5 mm, Irie) and mechanically homogenized for 2 min at 30 oscillations per second by a TissueLyser II apparatus (Qiagen). Total RNA was isolated from the resulting suspensions according to the manufacturer's procedure. Gene expression was evaluated by a 2-step quantitative RT-PCR method. Reverse-transcription of RNA samples was performed by using a High Capacity cDNA Reverse-Transcription Kit (Applied Biosystems), and quantitative PCR was performed by TaqMan(R) Fast Universal PCR Master Mix (Applied Biosystems). The mRNA levels of target genes were normalized to the GAPDH mRNA level. For murine apoC-III and GAPDH mRNA quantitation, TaqMan Gene Expression Assay IDs of Mm00445670_m1 and Mm99999915_g1 were used.

ELISA method for AON quantification in liver

Materials and reagents. The template DNA was a 25-mer DNA (5′-gaa tag cga taa taa agc tgg ata a-3′), which is complementary to **ON-9S** to **ON-15S**, with biotin at the 3′-end. The ligation probe DNA was a 9-mer DNA (5′-tcgctattc-3′) with phosphate at the 5′-end and digoxigenin at the 3′-end. The template DNA and the ligation probe DNA were purchased from Japan Bio Service. Reacti-Bind NeutrAvidin-coated polystyrene strip plates were purchased from Thermo Fisher Scientific (Nunc immobilizer streptavidin F96 white, 436015). The template DNA solution (100 nM) was prepared in hybridization buffer containing 60 mM Na_2HPO_4 (pH 7.4), 0.9 M NaCl, and 0.24% Tween 20. The ligation probe DNA solution (200 nM) was prepared in 1.5 units per well of T4 DNA ligase (TaKaRa) with 66 mM Tris-HCl (pH 7.6), 6.6 mM $MgCl_2$, 10 mM DTT and 0.1 mM ATP.

The washing buffer used throughout the assay contained 25 mM Tris-HCl (pH 7.2), 0.15 M NaCl and 0.1% Tween 20. Anti-digoxigenin-AP antibody (Fab fragments conjugated with

alkaline phosphatase) was obtained from Roche Diagnostics. A 1 : 2000 dilution of the antibody with 1 : 10 super block buffer in TBS (Pierce) was used in the assay. The alkaline phosphatase luminous substrate was prepared in 250 μM CDP-Star (Roche) with 100 mM Tris-HCl (pH 7.6) and 100 mM NaCl.

Assay procedures. Frozen liver tissue was collected in a 2 mL tube with 1 mL of PBS and a zirconia ball (∅ 5 mm, Irie) and mechanically homogenized for 2 min at 30 oscillations per second by a TissueLyser II apparatus (Qiagen). Total protein concentrations were measured using a detergent compatible assay kit (Bio-Rad) and adjusted to 8 mg L^{-1} with PBS. The assay was performed at the concentration range of 128 pM to 1000 nM in duplicate. For the standard curve, 7 standard solutions were prepared. To AON-untreated mice liver homogenates were added **ON-10S, ON-11S, ON-12S, ON-13S, ON-14S,** and **ON-15S** solutions to prepare 7 standard samples at a range of 128 pM to 1000 nM. Next, the template DNA solution (100 μL) and standard solution (10 μL) or liver homogenates (10 μL) containing **ON-10S, ON-11S, ON-12S, ON-13S, ON-14S,** and **ON-15S** were added to Reacti-Bind Neutr Avidin-coated polystyrene strip 96-well plates and incubated at 37 °C for 1 h to allow the binding of biotin to streptavidin-coated wells and hybridization. After hybridization, the plate was washed three times with 200 μL of washing buffer. Then, ligation probe DNA solution (100 μL) was added, and the plate was incubated at room temperature (15 °C) for 3 h. The plate was then washed three times with the washing buffer. Subsequently, 200 μL of a 1 : 2000 dilution of anti-digoxigenin-AP was added, and the plate was incubated at 37 °C for 1 h. After washing three times with the washing buffer, the CDP-Star solution was added to the plate, and finally the luminescence intensity was determined by using a Centro XS^3 luminometer (Berthold) one second after the addition of CDP-Star. The linear range of 128 pM to 1000 nM in this ELISA system was determined as $r > 0.97$.

Serum chemistry

Serum from the blood collected from the inferior vena cava upon sacrifice was subjected to serum chemistry. Assay kits (WAKO) were used to measure serum levels of aspartate aminotransferase (AST) and alanine aminotransferase (ALT), which are biomarkers for hepatic toxicity.

Statistics

Statistical comparisons were performed by Dunnett's multiple comparison tests. $*P < 0.05$, $**P < 0.01$, and $***P < 0.001$ were considered to be statistically significant in all cases. N.S. indicates no statistical significance.

Acknowledgements

A part of this work was supported by Basic Science and Platform Technology Program for Innovative Biological Medicine from the Ministry of Education, Culture, Sports, Science and Technology in Japan, JSPS KAKENHI Grant Number 24890102, Grants-in Aid for Scientific Research from the Japanese Ministry of Health, Labor, and Welfare (H23-seisaku tansaku-ippan-004 and H26-kanjitu-kanen-wakate-008) and the Advanced Research for Medical Products Mining Programme from the National Institute of Biomedical Innovation. T.Y. thanks the Grant for Research on Atherosclerosis Update from the Japan Heart Foundation & Astellas/Pfizer. A. Y. thanks the Research Fellowship from the Japan Society for the Promotion of Science (JSPS) for Young Scientists.

Notes and references

1 (*a*) E. R. Rayburn and R. Zhang, *Drug Discovery Today*, 2008, **13**, 513; (*b*) T. Yamamoto, M. Nakatani, K. Narukawa and S. Obika, *Future Med. Chem.*, 2011, **3**, 339.

2 (*a*) S. Obika, D. Nanbu, Y. Hari, K. Morio, Y. In, T. Ishida and T. Imanishi, *Tetrahedron Lett.*, 1997, **38**, 8735; (*b*) S. K. Singh and J. Wengel, *Chem. Commun.*, 1998, 1247.

3 (*a*) T. Yamamoto, M. Harada-Shiba, M. Nakatani, S. Wada, H. Yasuhara, K. Narukawa, K. Sasaki, M. A. Shibata, H. Torigoe, T. Yamaoka, T. Imanishi and S. Obika, *Mol. Ther. Nucleic acids*, 2012, **1**, e22; (*b*) K. Fluiter, A. L. ten Asbroek, M. B. de Wissel, M. E. Jakobs, M. Wissenbach, H. Olsson, O. Olsen, H. Oerum and F. Baas, *Nucleic Acids Res.*, 2003, **31**, 953; (*c*) K. Fluiter, M. Frieden, J. Vreijling, C. Rosenbohm, M. B. De Wissel, S. M. Christensen, T. Koch, H. Orum and F. Baas, *ChemBioChem*, 2005, **6**, 1104; (*d*) E. M. Straarup, N. Fisker, M. Hedtjarn, M. W. Lindholm, C. Rosenbohm, V. Aarup, H. F. Hansen, H. Orum, J. B. Hansen and T. Koch, *Nucleic Acids Res.*, 2010, **38**, 7100.

4 (*a*) R. S. Geary, E. Wancewicz, J. Matson, M. Pearce, A. Siwkowski, E. Swayze and F. Bennett, *Biochem. Pharmacol.*, 2009, **78**, 284; (*b*) M. J. Graham, S. T. Crooke, D. K. Monteith, S. R. Cooper, K. M. Lemonidis, K. K. Stecker, M. J. Martin and R. M. Crooke, *J. Pharmacol. Exp. Ther.*, 1998, **286**, 447.

5 (*a*) E. E. Swayze, A. M. Siwkowski, E. V. Wancewicz, M. T. Migawa, T. K. Wyrzykiewicz, G. Hung, B. P. Monia and C. F. Bennett, *Nucleic Acids Res.*, 2007, **35**, 687; (*b*) E. P. van Poelgeest, R. M. Swart, M. G. Betjes, M. Moerland, J. J. Weening, Y. Tessier, M. R. Hodges, A. A. Levin and J. Burggraaf, *Am. J. Kidney Dis.*, 2013, **62**, 796.

6 (*a*) O. Nakagawa, X. Ming, L. Huang and R. L. Juliano, *J. Am. Chem. Soc.*, 2010, **132**, 8848; (*b*) T. P. Prakash, M. J. Graham, J. H. Yu, R. Carty, A. Low, A. Chappell, K. Schmidt, C. G. Zhao, M. Aghajan, H. F. Murray, S. Riney, S. L. Booten, S. F. Murray, H. Gaus, J. Crosby, W. F. Lima, S. L. Guo, B. P. Monia, E. E. Swayze and P. P. Seth, *Nucleic Acids Res.*, 2014, **42**, 8796; (*c*) J. Winkler, *Ther. Delivery*, 2013, **4**, 791.

7 (*a*) S. M. A. Rahman, S. Seki, S. Obika, H. Yoshikawa, K. Miyashita and T. Imanishi, *J. Am. Chem. Soc.*, 2008, **130**, 4886; (*b*) P. P. Seth, A. Siwkowski, C. R. Allerson,

G. Vasquez, S. Lee, T. P. Prakash, E. V. Wancewicz, D. Witchell and E. E. Swayze, *J. Med. Chem.*, 2009, **52**, 10; (*c*) T. P. Prakash, A. Siwkowski, C. R. Allerson, M. T. Migawa, S. Lee, H. J. Gaus, C. Black, P. P. Seth, E. E. Swayze and B. Bhat, *J. Med. Chem.*, 2010, **53**, 1636; (*d*) P. P. Seth, C. R. Allerson, A. Berdeja, A. Siwkowski, P. S. Pallan, H. Gaus, T. P. Prakash, A. T. Watt, M. Egli and E. E. Swayze, *J. Am. Chem. Soc.*, 2010, **132**, 14942; (*e*) P. P. Seth, G. Vasquez, C. A. Allerson, A. Berdeja, H. Gaus, G. A. Kinberger, T. P. Prakash, M. T. Migawa, B. Bhat and E. E. Swayze, *J. Org. Chem.*, 2010, **75**, 1569; (*f*) K. Miyashita, S. M. A. Rahman, S. Seki, S. Obika and T. Imanishi, *Chem. Commun.*, 2007, 3765.

8 J. Lietard and C. J. Leumann, *J. Org. Chem.*, 2012, 77, 4566.

9 A. Yahara, A. R. Shrestha, T. Yamamoto, Y. Hari, T. Osawa, M. Yamaguchi, M. Nishida, T. Kodama and S. Obika, *ChemBioChem*, 2012, **13**, 2513.

10 (*a*) M. W. Johannsen, L. Crispino, M. C. Wamberg, N. Kalra and J. Wengel, *Org. Biomol. Chem.*, 2011, **9**, 243; (*b*) S. K. Singh, R. Kumar and J. Wengel, *J. Org. Chem.*, 1998, **63**, 6078; (*c*) M. D. Sorensen, M. Petersen and J. Wengel, *Chem. Commun.*, 2003, 2130.

11 K. Mori, T. Kodama, T. Baba and S. Obika, *Org. Biomol. Chem.*, 2011, **9**, 5272.

12 (*a*) Y. Mitsuoka, T. Kodama, R. Ohnishi, Y. Hari, T. Imanishi and S. Obika, *Nucleic Acids Res.*, 2009, **37**, 1225; (*b*) M. Nishida, T. Baba, T. Kodama, A. Yahara, T. Imanishi and S. Obika, *Chem. Commun.*, 2010, **46**, 5283; (*c*) K. Morita, M. Takagi, C. Hasegawa, M. Kaneko, S. Tsutsumi, J. Sone, T. Ishikawa, T. Imanishi and M. Koizumi, *Bioorg. Med. Chem.*, 2003, **11**, 2211; (*d*) Y. Liu, J. Xu, M. Karimiahmadabadi, C. Zhou and J. Chattopadhyaya, *J. Org. Chem.*, 2010, **75**, 7112; (*e*) A. R. Shrestha, Y. Kotobuki, Y. Hari and S. Obika, *Chem. Commun.*, 2014, **50**, 575.

13 M. Egli, G. Minasov, M. Teplova, R. Kumar and J. Wengel, *Chem. Commun.*, 2001, 651.

14 T. Yamamoto, S. Obika, M. Nakatani, H. Yasuhara, F. Wada, E. Shibata, M. A. Shibata and M. Harada-Shiba, *Eur. J. Pharmacol.*, 2014, **723**, 353.

15 T. Yamamoto, N. Fujii, H. Yasuhara, S. Wada, F. Wada, N. Shigesada, M. Harada-Shiba and S. Obika, *Nucleic Acid Ther.*, 2014, **24**, 283.

16 (*a*) T. Yamamoto, M. Harada-Shiba, M. Nakatani, S. Wada, H. Yasuhara, K. Narukawa, K. Sasaki, M. A. Shibata, H. Torigoe, T. Yamaoka, T. Imanishi and S. Obika, *Mol. Ther. Nucleic Acids*, 2012, 1; (*b*) R. Z. Yu, B. Baker, A. Chappell, R. S. Geary, E. Cheung and A. A. Levin, *Anal. Biochem.*, 2002, **304**, 19.

Removal of Plasma Mature and Furin-Cleaved Proprotein Convertase Subtilisin/Kexin 9 by Low-Density Lipoprotein-Apheresis in Familial Hypercholesterolemia: Development and Application of a New Assay for PCSK9

Mika Hori, Mitsuaki Ishihara, Yumiko Yuasa, Hisashi Makino, Koji Yanagi, Tamiko Tamanaha, Ichiro Kishimoto, Takeshi Kujiraoka, Hiroaki Hattori, and Mariko Harada-Shiba

Department of Molecular Innovation in Lipidology (M.H., Y.Y., M.H-S.), National Cerebral and Cardiovascular Center Research Institute, 5-7-1 Fujishirodai, Suita, Osaka 565-8565, Japan; Advanced Medical Technology and Development Division (M.I., T.K., H.H.), BML, Inc., 1361-1 Matoba, Kawagoe, Saitama 350-1101, Japan; Department of Endocrinology and Metabolism (H.M., T.T., I.K.), National Cerebral and Cardiovascular Center, 5-7-1 Fujishirodai, Suita, Osaka 565-8565, Japan; and Department of Cardiology (K.Y.), Kenporen Osaka Central Hospital, Umeda 3-3-30, Kita-ku, Osaka 530-0001, Japan.

Context: Proprotein convertase subtilisin/kexin 9 (PCSK9) is known to be a good target to decrease LDL cholesterol (LDL-C) and two forms of PCSK9, mature and furin-cleaved PCSK9, circulate in blood. However, it has not been clarified whether and how the levels of each PCSK9 are affected by LDL-apheresis (LDL-A) treatment, a standard therapy in patients with severe forms of familial hypercholesterolemia (FH).

Objective: Our objective was to investigate the differences in LDL-A-induced reduction of mature and furin-cleaved PCSK9 between homozygous and heterozygous FH, and between dextran sulfate (DS) cellulose adsorption and double membrane (DM) columns and to clarify the mechanism of their removal.

Design: A sandwich ELISA to measure two forms of PCSK9s using monoclonal antibodies was developed. Using the ELISA, PCSK9 levels were quantified before and after LDL-A with DS columns in 7 homozygous and 11 heterozygous FH patients. A crossover study between the two column types was performed. The profiles of PCSK9s were analyzed after fractionation by gel filtration chromatography. Immunoprecipitation of apolipoprotein B (apoB) in FH plasma was performed.

Results: Both mature and furin-cleaved PCSK9s were significantly decreased by 55–56% in FH homozygotes after a single LDL-A treatment with DS columns, and by 46–48% or 48–56% in FH heterozygotes after treatment with DS or DM columns. The reduction ratios of LDL-C were strongly correlated with that of PCSK9 in both FH homozygotes and heterozygotes. In addition, more than 80% of plasma PCSK9s were in the apoB-deficient fraction and a significant portion of mature PCSK9 was bound to apoB, as shown by immunoprecipitation.

Conclusions: Both mature and furin-cleaved PCSK9s were removed by LDL-A in homozygous and heterozygous FH either by binding to apoB or by other mechanisms. The ELISA method to measure both forms of plasma PCSK9 would be useful for investigating physiological or pathological roles of PCSK9. (*J Clin Endocrinol Metab* 100: E41–E49, 2015)

ISSN Print 0021-972X ISSN Online 1945-7197
Printed in U.S.A.

Received July 30, 2014. Accepted October 7, 2014.
First Published Online October 14, 2014

Abbreviations: DM, double membrane; DS, dextran sulfate; HDL, high-density lipoprotein; LDL, low-density lipoprotein; LDL-A, LDL-apheresis; LDL-C, LDL cholesterol; LDLR, low-density lipoprotein receptor; PCSK9, proprotein convertase subtilisin/kexin type 9; rh, recombinant human; TG, triglyceride.

Familial hypercholesterolemia (FH) is an inherited disorder caused by mutations in the low-density lipoprotein (LDL) receptor (LDLR), apolipoprotein B (apoB) or proprotein convertase subtilisin/kexin type 9 (PCSK9) (1, 2), and is characterized by high LDL cholesterol (LDL-C) levels leading to premature coronary artery disease (CAD). PCSK9, a serine protease, regulates plasma LDL-C levels by regulating degradation of LDLR (3, 4). It has also been reported that serum PCSK9 levels were significantly higher in FH patients than in controls (5), and were correlated with serum LDL-C levels (6).

PCSK9 encodes a 692-amino-acid protein composed of a signal peptide, a prodomain, catalytic, and C-terminal domains. It undergoes autocatalytic intramolecular processing to form a ~14-kDa prodomain and a ~60-kDa moiety with catalytic and C-terminal domains. Mature PCSK9 is composed of the prodomain, which is noncovalently attached to the catalytic domain. Another proprotein convertase, furin, cleaves PCSK9 at the Arg^{218}-Gln^{219} peptide bond, and the cleaved PCSK9 includes a ~7-kDa domain, ~14-kDa prodomain, and ~53-kDa domain (furin-cleaved form) that lacks the Ser^{153}-Arg^{218} segment (7, 8). It has been reported that furin-cleaved PCSK9 has no activity (7–9) to regulate LDLR and serum LDL-C or less activity than mature PCSK9 (10). Thus, it is important to measure both forms of PCSK9 separately, in order to clarify the significance of furin-cleaved PCSK9. However, no specific method has been reported for quantifying furin-cleaved PCSK9, and thus the association of the ratio of each form of PCSK9 with various pathological or physiological conditions, such as primary hyperlipidemia, hyperlipidemia in type II diabetes, obesity, etc., has not been clarified.

LDL-apheresis (LDL-A) treatment is a standard therapy in homozygous and severe forms of heterozygous FH. In order to selectively remove LDL, LDL adsorption techniques using dextran sulfate (DS) cellulose adsorption columns and double membrane (DM) filtration methods were developed (11, 12). We and other colleagues have reported that LDL-A reduces not only atherogenic lipoproteins, but also various proteins including coagulation factors and C-reactive protein (CRP), in serum (13–15).

Recently, it has been reported that PCSK9 was eliminated by LDL-A treatment in 6 FH patients (16). However, in FH homozygotes, the serum PCSK9 levels have been reported to be unaffected by LDL-A (17). Thus, the difference in the treatment-induced reduction of PCSK9 between FH homozygotes and heterozygotes has not been clarified. In addition, the differences in the PCSK9 reduction between DS and DM columns and between the mature and furin-cleaved forms have not been clarified. In the present study, we use a novel sandwich ELISA to measure the mature and furin-cleaved forms of PCSK9 and show that both forms were removed by LDL-A treatment in FH homozygotes and heterozygotes. Furthermore, the mechanism of their removal is also discussed.

Materials and Methods

Detailed materials and methods are shown in the Supplemental Materials and Methods.

Patient characteristics

The subjects were 18 FH patients, including 7 homozygotes and 11 heterozygotes, who were receiving either regular or an initial LDL-A treatment at either the National Cerebral and Cardiovascular Center Hospital or Kenporen Osaka Central Hospital from March 2009 to October 2013. They were diagnosed with homozygous or heterozygous FH using previously described criteria (18, 19). Among the patients who had undergone genetic testing (n = 12), the majority were found to have LDLR gene mutations (n = 6; 50%), and one had mutations of both the LDLR and PCSK9 genes. One patient had homozygous forms of LDL receptor adaptor protein 1 (LDLRAP1) gene mutation, and 5 patients had no mutation on either the LDLR, PCSK9, or LDLRAP1 genes (42%) (20). The backgrounds of the patients are summarized in Supplemental Table 1. The protocol of this study was approved by the Ethics Review Committee of the National Cerebral and Cardiovascular Center (M20–26). Each patient gave written informed consent to participate in the study. All clinical investigations were conducted in accordance with the principles of the Declaration of Helsinki.

LDL-apheresis

For LDL-A treatment, an instrument (MA-03®; Kaneka) with a plasma filter (Sulflux; Kaneka) and two DS columns (Liposorber LA-15®; Kaneka) to adsorb apoB-containing lipoproteins were used. A crossover study between DS and DM columns was performed in 5 FH heterozygotes (patients No. 8, 10, 11, 12, 14 in Supplemental Table 1). LDL-A by DM columns was performed using an instrument (KPS-8800Ce; Asahi Kasei Medical Co., Ltd.) with a plasma separator (Plasmaflow OP-05W; Asahi Kasei Medical Co., Ltd.) and a plasma fractionator (Cascadeflow EC-50W; Asahi Kasei Medical Co., Ltd.).

Plasma sample collections and assays

Peripheral blood was collected from the blood removal line immediately before and after a single LDL-A procedure. Plasma levels of total cholesterol (TC), triglyceride (TG), and high-density lipoprotein (HDL)-C were measured using enzymatic methods (Sekisui Medical Co.) and an automated analyzer (Hitachi Labospect 008, Hitachi-Hitec). Plasma Lipoprotein(a) (Lp(a)) levels were measured using a latex agglutination method (Sekisui Medical Co.). LDL-C levels were calculated by the Friedewald formula. Apolipoproteins levels were determined by turbidimetric immunoassay (LSI Medience Coorporation).

Construction, expression, and purification of recombinant PCSK9 proteins

Human PCSK9 cDNA was obtained by RT-PCR from mRNA of HepG2 cells and a C-terminal His_6 tag was added as described

(21). Briefly, PCR was carried out for mature PCSK9 (1–692 aa), and Δ218PCSK9 (219–692 aa), which corresponds to the furin-cleaved PCSK9. The respective cDNAs were subcloned into the pEF321 mammalian expression vector to yield pEF321/PCSK9 or pEF321/Δ218PCSK9 vector. CHO-K1 cells stably transfected with each vector were cultured. The mature form of recombinant human (rh) PCSK9 (rhPCSK9) from the culture medium was partially purified. For rhΔ218PCSK9, transfectant cells were collected by trypsinization, and suspended in TBS containing 1% NP-40. After centrifugation of the cell suspension, the supernatant was collected and used as a calibrator for furin-cleaved PCSK9 ELISA.

Production of monoclonal antibodies against PCSK9

Balb/c mice were immunized using a DNA-based or standard immunization method with 25 μg purified rhPCSK9 (21), and spleen cells from mice were fused with Sp2/0 myeloma cells. The supernatants of hybridoma cells were screened by ELISA using plates coated with purified rhPCSK9 (100 ng/well) and by immunoblotting. The specificities of each monoclonal antibody (Mab) obtained by standard immunization (1FB) and by DNA-based immunization (B1G, B12E, and G12D), respectively, were confirmed by ELISA and immunoblotting against purified rhPCSK9.

Measurement of plasma mature and furin-cleaved PCSK9 concentrations

Plasma mature and furin-cleaved PCSK9s were measured by an ELISA using a specific combination of Mabs as previously described (Supplemental Figure 1) (21). The absorbance was measured at 450 nm with a microplate reader.

Gel filtration chromatography

Gel filtration chromatography was performed on an AKTA purifier system (GE Healthcare). Plasma samples of 2 homozygous and 6 heterozygous FH patients were injected into two connected Superose 6 (1.0 × 30; GE Healthcare) columns (22). Cholesterol or Lp(a) was measured in the fractions using a BIO-Lis24 analyzer (Tokyo Boeki Medical System, Ltd.) or a Mercodia Lp(a) ELISA (Mercodia AB) with two Mabs against Apo(a) in accordance with the manufacturers' instructions. PCSK9s in the collected fractions were measured using the ELISA as described above.

Co-immunoprecipitation of apoB from FH plasma

A 500 μL plasma sample was adjusted to a final concentration of 50 mM HEPES [pH 7.4], 2.5 mM magnesium chloride, 1% Triton X-100, 0.5% sodium deoxycholate and protease inhibitor cocktail in a final volume of 1 mL. Samples were rotated at 4°C for 30 min, then centrifuged at 15 000 rpm for 15 min. Co-immunoprecipitation experiments were performed using a Pierce Co-Immunoprecipitation Kit (Pierce) following the manufacturer's instructions. The supernatants were applied to columns containing 20 μg of monoclonal anti-apoB antibody (Santa Cruz Biotechnology Inc.) or 20 μg of purified IgG from a nonimmunized mouse (Santa Cruz Biotechnology Inc.). The immunoprecipitates were separated by SDS-PAGE, followed by immunoblotting with monoclonal anti-apoB antibody (R&D Systems) or polyclonal PCSK9 antibody (R&D Systems). The bands were detected with ECL prime (GE Healthcare).

Statistical analysis

The statistical significance of differences between before and after LDL-A treatment was determined by the paired *t*-test. One-way ANOVA and Tukey's test were used to assess differences between groups. Spearman correlation analysis and linear regression were used to examine the relationship between PCSK9 reduction and LDL-C or HDL-C reduction. Values of $P < .05$ were considered to be statistically significant. All statistical analyses were carried out using the JMP software package (SAS Institute Inc.).

Results

Characterization of anti-PCSK9 Mabs

Purified rhPCSK9 was confirmed by SDS-PAGE followed by silver staining or by immunoblotting (Figure 1, A and B). The reactivity of Mabs to rhPCSK9 (mature form) was examined by SDS-PAGE under a nonreducing or reducing condition and by immunoblotting; Mabs 1FB, B1G, and B12E reacted with the 60-kDa mature PCSK9, while Mab G12D reacted with a 14-kDa prodomain of PCSK9 (Figure 1C). These three Mabs did not react with the mature segment of rhPCSK9 under a reducing condition. Similarly, the reactivity of all Mabs with native PCSK9 in human plasma was examined by immunoprecipitation. The 60-kDa mature PCSK9 and the 14-kDa prodomain of PCSK9 were co-immunoprecipitated with Mabs 1FB, B12E, and G12D, while the 53-kDa furin-cleaved PCSK9 alone was precipitated with Mab B1G (Figure 1, D and E).

Standardization of ELISA for the mature and furin-cleaved PCSK9s in plasma

We have established three different sandwich ELISAs specific for plasma total, mature and furin-cleaved PCSK9s (Supplemental Figure 1). Each system showed a dose-dependent response to purified rhPCSK9 or cell lysate of rhΔ218PCSK9 as well as to plasma samples, and the reactivity profiles were equivalent with both recombinant and plasma PCSK9 (Supplemental Figure 2). Calibration curves in the ELISA for total and mature PCSK9, rhPCSK9 protein, as a primary calibrator and rhPCSK9 culture medium, as a secondary calibrator were obtained (Supplemental Figure 3). Similarly, the calibration curve was made using dilutions of the cell lysate of rhΔ218PCSK9 for furin-cleaved PCSK9.

Changes of plasma lipids and apolipoproteins between before and after LDL-A with DS columns in FH homozygotes or heterozygotes

In FH homozygotes, a single procedure of LDL-A treatment with DS columns produced 57–78% reduction in